

**Assessing Meadow Carbon Cycling Using Digital Repeat Photography and Eddy
Covariance Techniques**

A Thesis submitted to the faculty of
San Francisco State University
In partial fulfillment of
the requirements for
the Degree

Master of Arts

In

Geography: Resource Management and Environmental Planning

by

Shamim Mousavi

San Francisco, California

December 2021

Copyright by
Shamim Mousavi
2021

Certification of Approval

I certify that I have read *Assessing Meadow Carbon Cycling Using Digital Repeat Photography and Eddy Covariance Techniques* by Shamim Mousavi, and that in my opinion this work meets the criteria for approving a thesis submitted in partial fulfillment of the requirement for the degree Master of Arts in Geography: Resource Management and Environmental Planning at San Francisco State University.

Andrew Oliphant, Ph.D.
Professor,
Thesis Committee Chair

Sara Baguskas, Ph.D.
Assistant Professor

Assessing Meadow Carbon Cycling Using Digital Repeat Photography and Eddy Covariance Techniques

Shamim Mousavi
San Francisco, California
2021

Montane meadows of Sierra Nevada have strong seasonality in plant phenology and plant water availability which has a direct impact on the duration of the growing season and the carbon cycle of this ecosystem. Significant progress has been made recently linking phenological observations using digital repeat photography to carbon cycle rates for a variety of ecosystems. We used green chromatic coordinate (GCC), an algebraic combination of red, green and blue color channels to represent vegetation photosynthetic potential. We compared GCC with daily total carbon fluxes derived from eddy covariance (EC) observations for two meadows over different growing seasons. At a seasonal timescale, GCC closely matched the EC-derived carbon exchanges, with both datasets reflecting the phenological cycle of the ecosystem in detail. Based on these relationships, we derived empirical models for different carbon fluxes and different meadow-seasons. Model performance varied between fluxes and meadows and phenological stages but shows promising results, with an R^2 value of 0.74 for modeled versus observed daily gross primary production (Nash Sutcliffe model efficiency coefficient ((NS-MEC) =0.74). The model for net ecosystem production was more consistent between meadow-years with an overall model $R^2=0.91$, NS-MEC=0.91.

Acknowledgements

I want to thank professor Andrew Oliphant and professor Sara Baguskas, my committee, for their support and guidance during writing of my thesis. I also thank all the professors and lecturers in the Department of Geography & Environment who helped me during my undergraduate and graduate journey. This project was funded by the California Climate Investments and California Department of Fish and Wildlife Wetlands Restoration for Greenhouse Gas Reduction fund and is a part of The Sierra Fund's Ecosystem and Community Resiliency in the Sierra Nevada: Restoration of the Clover Valley Ranch Project (grant agreement Q1996007). I would like to acknowledge the landowners Red Clover LLC and additional project partners that helped make this project possible, funding for the meadow restoration work came from the Natural Resource Conservation Service, the Wildlife Conservation Board, and the United States Fish and Wildlife Service. This project takes place on the traditional homelands of the Maidu. I also thank the SFSU meadow team for help in the field. I want to thank professor Richard Street for helping me to revise my thesis. Although words are not enough, I thank my husband, Ali Iranpour, and my daughter, Arianna Iranpour, for their kindness, support, understanding and for giving me ambition to continue my education. I thank my parents in Iran whose kind words gave me hope for a brighter future. The Red Clover Valley and the Department of Geography & Environment with all its kind faculty and staff, will forever be one of the happiest places in my memory and my heart.

Table of Contents

Certification of Approval	iii
Acknowledgements	v
Table of Contents	vi
List of Tables	viii
List of Figures	ix
Introduction	1
1.1 Sierra Nevada Meadows Background and Montane Meadow Definition	1
1.2 Hydrology, Meadow’s Health and Water Table	2
1.3 Productivity of Sierra Nevada Meadow: Vegetation and Soil.....	4
1.4 History of Land Use and Land Use Management	8
1.5 Meadow Restoration.....	10
1.6 Meadow Ecological Services: Carbon Sequestering and Carbon Cycling	12
1.7 Phenology of Sierra Nevada Meadows	14
1.8 Use of Phenological Observations to Characterize Carbon Cycling.....	15
1.9 Research Objectives	16
1.10 Rationale for the Research	17
Study Site	19
2.1 Red Clover Valley Ranch Location, History and Land Degradation.....	19
2.2 Red Clover Valley Restoration Project and Management	21
2.3 Red Clover Valley Climate, Location of Towers and Study Time	22
Methodology	24
3.1 Digital Repeat Photography (DRP)	25
3.2 Green Chromatic Coordinate (GCC).....	26
3.3 Digital Repeat Photography Experimental Design	28
3.4 Photo Quality Control.....	30
3.5 Selecting the Region of Interest (ROI) and Data Processing.....	31
3.6 Eddy Covariance Technique and its Theory	33
3.7 Data Processing, Flux computation, Data correction and Rejection	34

3.8 CO ₂ Flux Partitioning and Gap-Filling.....	35
3.10 Eddy Covariance Experimental Design.....	36
3.11 Eddy Covariance Tower Footprint	39
Results	41
4.1 Seasonal Patterns.....	41
4.1.1 Seasonal Patterns in Observed CO ₂ Exchanges.....	41
4.1.2 Seasonal Patterns in GCC and RCC	43
4.2 Relationship Between Seasonal Patterns of GCC, and CO ₂ Exchanges	48
4.3 Characterizing Seasonal Patterns in the Relationship with GCC, GPP and NEP	49
4.4 Modeling GPP and NEP Using GCC	51
4.4.1 Growth Phase Model	52
4.4.2 Senescence Phase Model.....	56
4.4.3 Combined All-Seasons Models	60
Discussion	61
5.1 Water Availability and Vegetation Community Control on Carbon Exchange.....	62
5.2 Separating Phenophases and Choosing Seasonal Phases	64
5.3 GPP and GCC Relationship in Different Phenological Phases.....	65
5.4 GPP vs. NEP Modeling	66
Conclusion	68
References.....	72

List of Tables

Table 1: Most common plant species in hydric, mesic, and xeric Sierra Nevada Meadows	5
Table 2: Common model of camera used for digital repeat photography.....	26
Table 3: Camera type and specifications for each year of the study.....	29
Table 4: Comparison between eddy covariance towers	38
Table 5: List of instruments on the eddy covariance tower.....	38
Table 6: Regression equations and statistics for polynomial relationships between GCC and CO ₂ fluxes for growth phase, where NS-MEC is the Nash-Sutcliffe model efficiency coefficient.	54
Table 7: Regression equations and statistics for polynomial relationships between GCC and CO ₂ fluxes for senescence phase, where NS-MEC is the Nash-Sutcliffe model efficiency coefficient.	58

List of Figures

Figure 1: Sierra Nevada meadows across California. (Source: Viers et al., 2013)	2
Figure 2: Process of function of a healthy meadow. (Source: Viers et al., 2013)	3
Figure 3: Incision cycle due to altering hydrology. (Source: Viers et al., 2013).....	4
Figure 4: Conceptual model of major carbon movements in a meadow ecosystem (Adapted from: Oliphant et al., 2018).....	14
Figure 5: Location of Red Clover Valley Ranch, creeks and flux tower. (Source: Google Earth)	20
Figure 6: Climatology of study area. Thirty year (1981-2010) monthly average precipitation and monthly average minimum and maximum temperature for Portola, California. (Source: National Climate Data Center, NCDC).	23
Figure 7: Vegetation peak of growing season and senescence phase in Red Clover valley, 2019.	24
Figure 8: An example of a gray reference panel (red rectangle box), Red Clover Valley, August 2020.	31
Figure 9: Example of selecting ROI for Red Clover Valley meadow, June 03, 2019, at 11:00. The blue, red and yellow ROIs selection (a) for mesic and (b) for xeric plant community to represent the sample to extract digital numbers.....	32
Figure 10: Eddy covariance tower with its instruments, installed at Red Clover Valley meadow, Ca, October 2020.	39
Figure 11: RCV1 flux tower footprint using the Hsieh (2000) analytical model, computed by MATLAB, located in Red Clover Valley, CA, 2019.....	40
Figure 13: Seasonal pattern of green chromatic coordinate (GCC), of Loney Meadow in 2016, mesic and xeric communities of Red Clover Valley meadow (RCV1) in 2019 and RCV2 in 2020 and 2021.	43

Figure 14: Seasonal patterns of green chromatic coordinate (GCC) and red chromatic coordinate (RCC), of Loney Meadow in 2016, mesic community of Red Clover Valley meadow (RCV1) in 2019 and (RCV2-2021) in 2021.46

Figure 15: Seasonal patterns of (a) GCC and GPP, (b) GCC and NEP for Loney Meadow in 2016 and (c) GCC and GPP, (d) GCC and NEP for Red Clover Valley meadow (RCV1) in 2019.48

Figure 16: Growth phase and senescence phase for (a) daily GPP and GCC values and (b) NEP and GCC values for Loney Meadow, 2016, and Red Clover Valley meadow (RCV1), 2019.49

Figure 17: (a) seasonal pattern of GPP and GCC, (b) senescence phase pattern of GPP and GCC, (c) relationship between GPP and GCC, (d) accuracy graph of modeled GPP for Red Clover Valley meadow (RCV1), 2019.51

Figure 18: (a) GPP regression models based on GCC values (b) NEP regression models based on GCC values for Loney Meadow, 2016, Red Clover Valley meadow (RCV1), 2019, and all-meadows, for growth phase.52

Figure 19: (a) GPP regression models based on GCC values, (b) NEP regression models based on GCC values for Loney Meadow, 2016, Red Clover Valley meadow (RCV1), 2019, and all-meadows, for senescence phase.56

Figure 20: (a) combined all-seasons GPP modeled values accuracy and (b) combined all-seasons NEP modeled values accuracy, against observed carbon fluxes with eddy covariance for Loney Meadow, 2016, and Red Clover Valley meadow, RCV1, 2019.60

Introduction

Montane meadows are unique biophysical systems with inextricable links between geomorphic, hydrologic and biological processes. They generate a unique seasonal wetland ecosystem, provide mountain biodiversity hotspots and numerous ecological services such as water quality and flow control and the capture and storage of atmospheric CO₂ (Viers et al, 2013; Blackburn et al, 2021). These following sections introduce the biophysical characteristics of montane meadows of the Sierra Nevada in California, with special focus on carbon cycling and vegetation phenology. At the conclusion, the research objectives and rationale for this study will be presented.

1.1 Sierra Nevada Meadows Background and Montane Meadow Definition

Mountain meadows of the Sierra Nevada produce ecosystems defined by biotic and abiotic characteristics such as vegetation, soil and hydrology. According to Viers et al., (2013), there are 17,039 meadows in the Sierra Nevada that are not uniformly distributed across the range, covering 191,900 acres (77,659 hectares) (Figure 1). Sierra Nevada meadows can be classified based on their wetness, range type, vegetation type, geomorphic, hydrology and altitude (Ratliff, 1985). One category of meadows are montane meadows that have characteristics composed of one or more plant communities consisting of herbaceous species, flat and low gradients valleys of watersheds that have shallow and impermeable soil with high water tables (Pope et al., 2015; Debinski et al., 2000; Weixelman et al., 2011). Montane meadows often produce wetlands or semi wetlands at elevations of more than 500 m with shallow groundwater (<1 m depth) and fine textured soil supporting different types of vegetation of subalpine and alpine zones (Viers et al., 2013). Montane meadows can occur as result of patch disturbances

such as fire, glacier movement, natural geomorphic processes, or animal disturbances such as beaver dam meadows (Debinski et al., 2000).

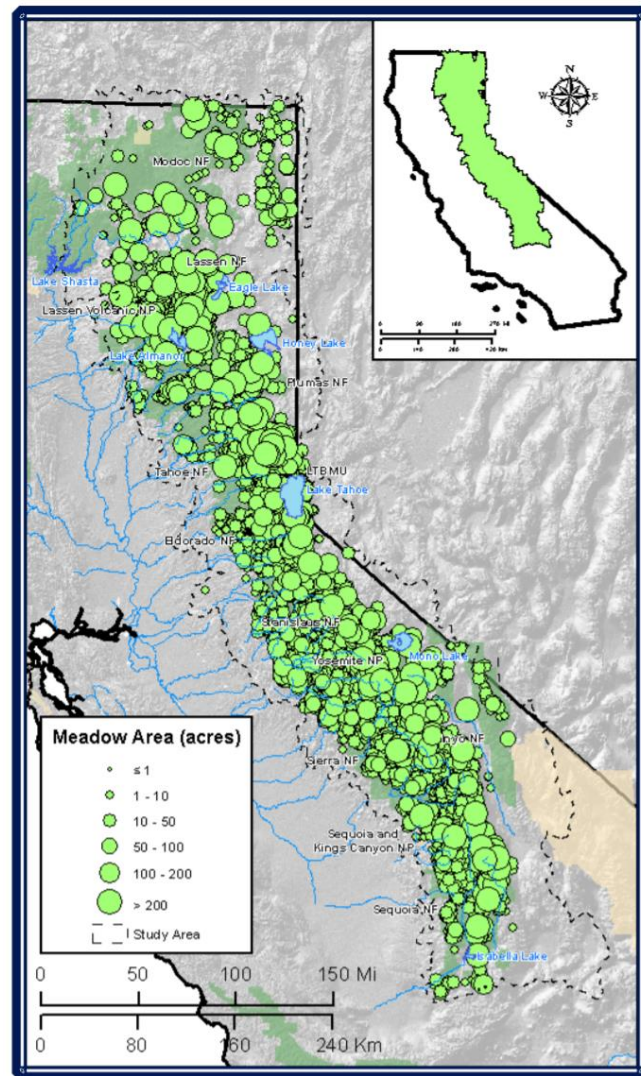


Figure 1: Sierra Nevada meadows across California. (Source: Viers et al., 2013)

1.2 Hydrology, Meadow's Health and Water Table

Montane meadows have four primary water sources: snowmelt, overland flow within the basin, surface flow entering via stream and spring networks, and direct precipitation (Lord et al.,

2011). Meadows lose water through evaporation and surface outflow. Snow melt adds significantly to surface water and groundwater. This causes soil moisture and base flow to increase during late spring and early summer, which coincides with the peak of the growing season. It is important that snow melts gradually to maintain levels of saturation and a consistent ground water elevation (<1 m) (Viers et al., 2013). A high groundwater table supports hydrophilic meadow plants and higher transpiration rates (Loheide & Lundquist, 2009). Moreover, while high groundwater table sustains meadow plants, and periodic flooding helps to distribute surface water across the meadow. Hydric vegetation roots provide excellent bank stability and reduce channel incision (Viers et al., 2013). This results in channel resistance which leads to stable stream banks and amplifies overbank flooding, which causes additional groundwater recharge, the extension of baseflow, and the persistence of meadow vegetation (Figure 2).

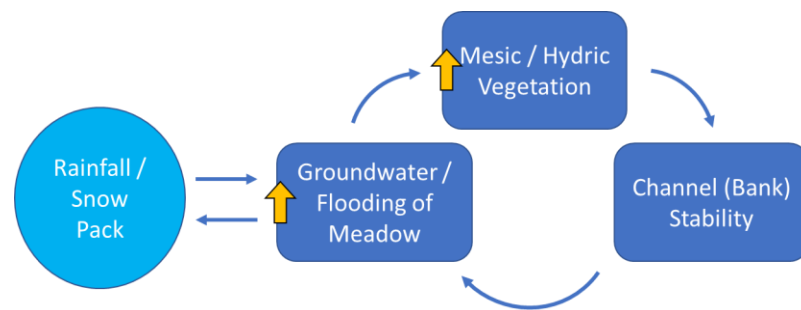


Figure 2: Process of function of a healthy meadow. (Source: Viers et al., 2013)

Anthropogenic activity, such as grazing and creating roads, causes a cycle of channel incision. Channel incision decreases the groundwater level and often results in a shift from hydrophilic to xeric vegetation. Loss of dense and fibrous roots of hydric vegetation exacerbates bank erosion and decreases channel stability, leading to further channel incision and reduction of

meadow flooding. As flows are more quickly conveyed downstream, groundwater levels also decrease (Schilling et al., 2004). Moreover, climate change and increase of air temperature causes precipitation to fall more as rainfall and less as snow, further enhancing the incision cycle and contributing to a decrease in groundwater level (Figure 3).

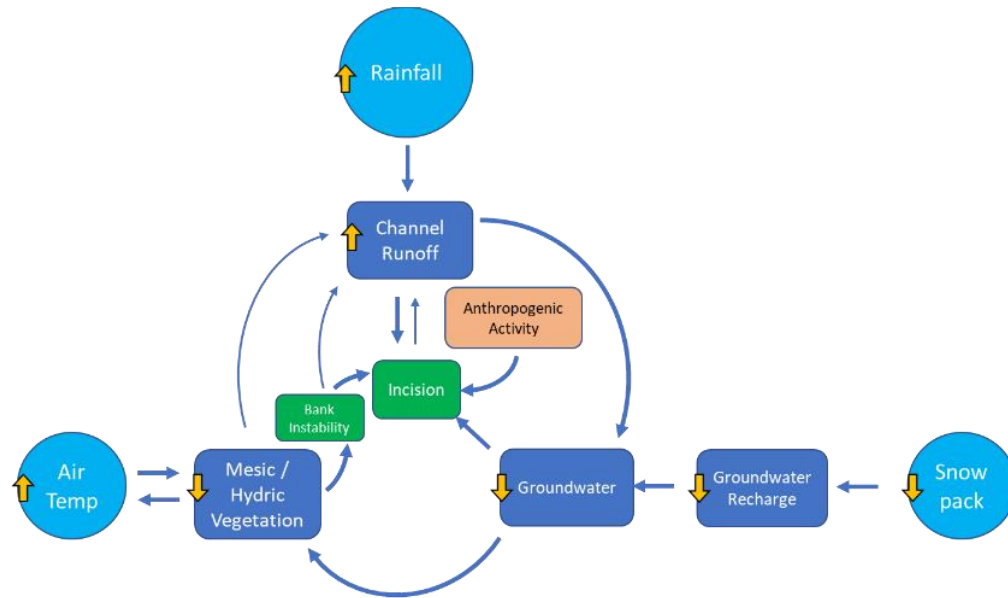


Figure 3: Incision cycle due to altering hydrology. (Source: Viers et al., 2013)

1.3 Productivity of Sierra Nevada Meadow: Vegetation and Soil

Productivity of Sierra Nevada meadows varies with complex and interacting factors, such as elevation, plant species, soil type (fertilization) and degree of grazing. However, the main driver of productivity in a meadow is presence or absence of near-surface water and the duration that water is available during the year (Weixelman et al., 2011). Meadow plant community composition largely reflects water availability and the depth of the water table (Dwire et al., 2006). On this basis, previous researchers have divided meadows into three categories (Dwire et al., 2006). The first, wet and moist meadows support both the hydric meadow community

(hydrophytes) dominated by sedge species, and the mesic meadow community (mesophytes) dominated by herbaceous perennial vegetation (Table 1). They also can include riparian shrubs such as willows (*Salix eastwoodiae*). Water table depth for hydric meadow community ranges from +26 cm (above soil surface) to -27 cm (below surface) and for mesic meadow community from +17cm to -73cm (Dwire et al., 2006). Dry meadows support xeric meadow communities dominated by sagebrush (*Artemisia tridentata*) that can dominate dry hillslopes (Chambers et al., 2004). Water table depth for xeric plant community ranges from -8cm to -115 cm (Dwire et al., 2006). Xeric plant community dominate degraded meadows as a direct result of drying of riparian areas, which is caused by draining of meadow sediments as a consequence of stream incision, over grazing, land use changes, and climate change (Loheide & Gorelick, 2007).

Table 1: Most common plant species in hydric, mesic, and xeric Sierra Nevada Meadows

Scientific name	Common name	Citation
Wet Meadow (hydric)		
<i>Aster occidentalis</i>	Western aster	Ratliff, 1982
<i>Carex nebrascensis</i>	Nebraska sedge	Ratliff, 1982; Maher 2015
<i>Carex utriculata</i> Boott	Northwestern sedge	Dwire et al., 2006
<i>Carex aquatilis</i> Wahl	Water sedge	Dwire et al., 2006
<i>Salix eastwoodiae</i>	Mountain willow	Lowry et al., 2011
<i>Carex angustata</i>	Narrow-leaved sedge	Clover Valley Ranch Vegetation Monitoring, 2018
<i>Carex filifolia</i> var <i>erostrata</i>	Threadleaf sedge	Clover Valley Ranch Vegetation Monitoring, 2018
<i>Carex simulate</i>	Short-beaked sedge	Clover Valley Ranch Vegetation Monitoring, 2018
<i>Ranunculus longirostris</i>	Water buttercup	Clover Valley Ranch Vegetation Monitoring, 2018
<i>Sidalcea oregana spicata</i>	spicate checker	Clover Valley Ranch Vegetation Monitoring, 2018
Moist Meadow (mesic)		
<i>Juncus balticus</i>	Grass/forbs	Dwire et al., 2006
<i>Poa protensis</i>	Bluegrass	Dwire et al., 2006; Ratliff, 1982
<i>Carex microptera</i>	Small wing sedge	Dwire et al., 2006

Scientific name	Common name	Citation
Moist Meadow (mesic)		
<i>Carex lanuginose</i>	Woolly sedge	Clover Valley Ranch Vegetation Monitoring, 2018
<i>Eleocharis cyperaceae</i>	Marsh dweller sedge	Clover Valley Ranch Vegetation Monitoring, 2018
<i>Scirpus cyperaceae</i>	Club rush	Clover Valley Ranch Vegetation Monitoring, 2018
<i>Anguina agrostris</i>	Bent grass	Clover Valley Ranch Vegetation Monitoring, 2018
<i>Deschampsia</i>	Hair grass	Clover Valley Ranch Vegetation Monitoring, 2018
<i>Danthonia</i>	Oat grass	Clover Valley Ranch Vegetation Monitoring, 2018
<i>Alopecurus aequalis</i>	Shortawn foxtail	Clover Valley Ranch Vegetation Monitoring, 2018
Dry Meadow (xeric)		
<i>Artemisia tridentata</i>	Big sagebrush	Ratliff, 1982; Maher 2015
<i>Artemisia arbusculata</i>	Dwarf sagebrush	Clover Valley Ranch Vegetation Monitoring, 2018
<i>Artemisia cana</i>	Silver sagebrush	Clover Valley Ranch Vegetation Monitoring, 2018
<i>Purshia Tridentate</i>	Bitterbrush	Clover Valley Ranch Vegetation Monitoring, 2018
<i>Chrysothamnus nanuseosus</i>	Rabitt brush	Clover Valley Ranch Vegetation Monitoring, 2018
<i>Danthonia California Boland</i>	California oat grass	Dwire et al., 2006
<i>Astragalus glaucus</i>	short-beaked agoseris	Clover Valley Ranch Vegetation Monitoring, 2018
<i>Pyrocoma lucida</i>	Sticky pyrocoma	Clover Valley Ranch Vegetation Monitoring, 2018
<i>Polemonium micranthum</i>	Annual sky pilot	Clover Valley Ranch Vegetation Monitoring, 2018
<i>Leucocrinum montanum</i>	Sand lily	Clover Valley Ranch Vegetation Monitoring, 2018

Soil moisture modifies meadow vegetation in predictable ways. A fine-textured soil draws water to shallow rooted meadow plants (Ratliff, 1985). Soil of Sierra Nevada meadows consist dominantly of alluvial deposits and less of glacial debris and free of rock deposits. They

are distinguished by their water regime, texture, stratification, and volcanic ash content. Meadow soil is rich in decayed organic matter and has a high water table that causes soil to become dark in color, fertile and mottled at depth. Mottling reflects the depth of the seasonal water table (Taskey, 1995). Montane meadow soil is wet because it is usually covered by snow in the winter and then receives snowmelt runoff and elevated groundwater during spring and early summer. However, in the Mediterranean climate dry summers of the Sierra Nevada, surface soils tend to desiccate from early summer through to the first rains in October/November. Also, as the soil texture is fine, has less rocks and more volcanic ash content, soil has more capacity to hold water. Wet and moist meadow soils may be permanently saturated at shallow depths. Wet meadow soil is gleyed soil which means it has dark, blue black color casing by chemical reduction of metallic compounds due to lack of oxygen (Taskey, 1995). In wet meadow soils, anaerobic activities occur from March to July at depths of 10 cm, and throughout the year at depths of 25 cm. In moist meadow soils, anaerobic activities happen only during spring and aerobic activity in summer and fall, while in dry meadow soils, aerobic activities occur throughout the year (Dwire et al., 2011).

Soil in the meadows that have been subjected to grazing, logging, wildfire, recreation and other land diversion can become compacted. This means soil has hardened surfaces, less porous, resistance to root penetration and decreased permeability to water and gases. These cause an increase in surface runoff and erosion, and decrease in gas exchange between atmosphere, plant roots and soil microorganisms (Taskey, 1995). The degree of compaction depends on the amount of pressure applied and soil characteristics such as texture, organic matter content and water content. Therefore, wet meadows as they have fine soil, with less rock and richer in ash content

are most easily damaged. Full recovery from compaction is not possible although partial recovery depends on biological activity, environmental factors such as freeze-thaw events and soil condition (Taskey, 1995).

1.4 History of Land Use and Land Use Management

The montane meadows of the Sierra Nevada have a long history of human intervention and exploitation that has accelerated and intensified in the last 200 years. It has been identified as one of the most altered, impacted and at-risk landscapes in the Sierra Nevada region (Keeley et al., 2003; Loheide et al., 2009). This has led to widespread ecosystem degradation in the form of erosion, incision, loss of water table, encroachment of xeric and non-native vegetation, loss of native species, and exacerbated disturbance regimes, such as catastrophic wildfire.

Overgrazing in the late 1800's and early 1900's resulted in widespread meadow deterioration. National Parks, United States Forest Service (USFS) and the Bureau of Land Management (BLM), have recorded the impact of livestock (Menke, 1996). In 1934, the Taylor Grazing Act established “grazing districts” and dictated a permitting system employed by all federal land management agencies. The Bureau of Land Management was charged with halting overgrazing and soil deterioration (Menke, 1996). As awareness of ecological impacts of overgrazing grew, from 1960 onwards, a set of prevention steps and improvement projects, such as enclosures, rest-rotation systems, erosion control structures, and replanting of native riparian species was introduced (Allen-Diaz, 1991; Menke, 1996).

During the mid-19th century, Sierra Nevada was the center of extensive gold mining. These mining activities impacted the geomorphology and continue to impact water quality across watersheds. There is an estimate of between 20,000 and 40,000 abandoned mines throughout the

Sierra Nevada region (James,1994). The impact of mining on meadows and watersheds further worsened with the introduction of hydraulic gold mining. This led to a rapid decline of health of the Sierra Nevada meadow ecosystems due to a significant increase in sediment production and widespread channel aggradation, which is still stored in significant quantities in watersheds of the Sierra Nevada (James,1994; Gilbert, 1917). Further, these mining practices led to numerous toxic chemicals, such as mercury and lead being released from the sediment, which directly affects the quality and distribution of aquatic species habitat.

Gold mining resulted in substantial increases in timber harvesting, which consumed huge amounts of timber for building tunnels, and rail beds for transporting the ore by train to the markets as well as used as fuel for ore processing (McKelevy & Johnston, 1992). Timber harvesting intensified during World Wars I and II, and to an even greater extent in the post WWII boom when increased housing construction created high demand for lumber. There are limited studies on the direct impact of timber harvesting on meadows, but the indirect effects include channel gullying and channel down-cutting due to increased rates of runoff and erosion associated with upslope harvested areas. Water management during the 20th century is yet another area affecting the Sierra Nevada meadows, which were further added to the set of impacts from earlier times. With the increased population and increased importance of agriculture, the need for redirecting and transporting Sierra Nevada water for irrigation and use by coastal urban areas increased substantially (Menke et al. 1996). All these activities have had substantial impact and pressure on the health of meadows in the Sierra Nevada.

In recent centuries, human land use and land cover change have contributed to anthropogenic climate change that has resulted in a 10–15% increase in atmospheric carbon

dioxide concentrations (Ciais et al., 2014). Since 1850, land type conversion, such as forest to cropland, and land degradation has resulted in a cumulative carbon loss of 490 Pg C (Mahowald et al., 2017). Specifically, 40% of the carbon loss is associated with land-use and land cover change and 60% is an indirect consequence of the loss of potential natural vegetation or carbon sinks (Mahowald et al., 2017). Therefore, implementing practices and restoration plans for converted and degraded lands is important, as these restored ecosystems can improve the rate that carbon dioxide is removed from the atmosphere, converted to plant material, and stored in soil as organic matter. In recent years in California, the increase in drought and wildfires has resulted in management approaches that address restoring degraded ecosystem. Also, The California Cap and Trade program has funded meadow restoration with the primary purpose of reducing State carbon emissions and enhancing carbon sequestration. An example is Fish and Wildlife Wetlands Restoration for Greenhouse Gas Reduction Program (Wetlands Restoration for Greenhouse Gas Reduction Program, 2018). This program has a focus on projects that lead to reduction of greenhouse gases in wetlands and watersheds in California as wetlands have high carbon sequestration capacity and can store carbon in the soil and vegetation for decades. Moreover, this program will enhance native vegetation growth and health, improve water quality and quantity, enhance soil stability and organic matter, and help California to reduce carbon emissions (Wetlands Restoration for Greenhouse Gas Reduction Program, 2018).

1.5 Meadow Restoration

Sierra Nevada meadows have been subjected to both changes in climate and morphological degradation due to primary human activity (Verma et al., 1989; Wohlfahrt et al., 2008). These changes impact the meadow morphology and hydrology as stream channels

decrease in meandering and straighten, which results in an increase in runoff from watersheds above the meadow resulting in less water filtration (Weiser, 2017). Changing in the streams cause the soil water content in the meadow surface to decrease, which impacts the productivity and distribution of vegetation (Figure 3).

In recent decades, different meadow restoration plans helped to increase ground water levels and enhance native vegetation. This is particularly important for the Sierra Nevada region as water needs in this region is great. Sierra Nevada snowmelt provides drinking water to local residents and also a portion of drinking water of 23 million people from the Bay Area to Southern California (Sierra Nevada Restoration, 2018). There are federal, state, local and private organizations with different restoration programs operating in this region. An example of restoration program includes the National Fish and Wildlife Foundation (NFWF), which has a goal of restoring about 8,090 hectares per year of the approximately 77,660 hectares of meadow habitat in the Sierra Nevada of California (Viers et al. 2013).

There are different meadow restoration types such as check dams, tilling and revegetation. A primary, common method is rewatering techniques such as pond-and-plug that has been applied to Knuthson meadow in Carmen Valley in Sierra Nevada (Maher, 2015). With help of this technique the meadow water table will raise and cause an increase in water storage, and maintains meadow hydric species, thereby increasing vegetative productivity and increasing carbon sequestration (Loheide et al. 2009). In this technique, meadow sediment is used to plug incised channels to divert flow onto the meadow floodplain. Blocking channel flow causes the water table to rise nearly immediately. However, this technique involves major land disturbance as excavating alluvial material from the incised channel and floodplain and using the material to

plug the incised channel. The result is a series of ponds and plugs that cover the previously incised meadow channels (Viers et al., 2013). The restoration plan also decreases sediment transportation downstream and increases biodiversity and habitat stability, retention of pollutants, and a steady release of water downstream (Viers et al., 2013; Loheide et al. 2009). Hammersmark et al. (2008) concluded that pond-and-plug restoration projects in northeastern California meadows had raised groundwater levels, increased the duration of flooding and decreased the magnitude of flood peaks.

Another technique for meadow restoration is Beaver Dam Analogue (BDA), one of the fastest stream restoration techniques (1 to 3 years) for deeply eroded streams (Goldfarb, 2018). BDAs are cheap compared to other restoration techniques such as pond-and-plug. BDAs are human made small dams at bottom of the damaged stream bed usually made with willow sticks that will attract beavers. After that, beavers constantly continue the stream restoration process by adding their own dams to the BDAs. Beavers and BDAs combat stream incision by promoting sediment deposition, allowing suspended particles to settle, slowing water velocity, diverting flows, and widening the incised channel (Bouwes, 2020; Goldfarb, 2018). As sediment accumulates, streams become less steep, and more hydrologically connected to the floodplain leading to a recharge of ground water and increase of the water table. Raising the water table irrigates willows as well as native mesic and hydric species. Also, the riparian corridor provides healthy habitat to a wide range of species (Bouwes, 2020; Goldfarb, 2018).

1.6 Meadow Ecological Services: Carbon Sequestering and Carbon Cycling

Meadows provide many ecological services, increase ecosystem resilience and biodiversity, support pollinator insects, enhance natural corridors, reduce soil erosion and

compaction by increasing in ground water recharge (Meadow Restoration, 2019). Meadows provide habitat and refuge for fish, amphibians, birds, and mammals; reduce flood flows; sustain base flows; and filter out water from undesirable constituents and sediment (Viers et al., 2011; Loheide et al., 2009). Meadows also support adjacent riparian ecosystems by stabilizing streambanks and shorelines and providing key pathways for hydrologic cycling (Hammersmark et al. 2008). Additionally, they provide ecological services to humans by regulating water flow, improving water quality, reducing air pollution through air filtration by vegetation.

Moreover, meadows contribute significantly to carbon sequestration and have a high capacity to be a carbon sink (Hirota et al., 2010). Globally, each year, meadow ecosystems can absorb 3.9 to 6.1 Gg of carbon (Verma et al., 1989; Baldocchi, 2008). However, deteriorating meadows release greenhouse gases into the atmosphere and can be a net source of carbon instead of acting as carbon sinks (Kayranli et al. 2010; Norton et al. 2011; Badiou et al. 2011).

Hydrologic controls on plant water availability, and other environmental controls on vegetation functioning (at diurnal, synoptic, seasonal, and interannual timescales) can control the health of a meadow and influence the shift between sink or source of carbon (Wever et al., 2002; Xu & Baldocchi, 2014; Wohlfahrt et al., 2008).

Based on Figure 4, carbon cycle approximation in a meadow is defined as:

$$\Delta S = GPP - RE \pm F_{CH_4} \pm F_G \pm F_W, \text{ (Eq. 1)}$$

where, ΔS is total carbon absorb (or release) through vegetation, organism and soil. GPP is gross primary production and is amount of photosynthesis done by vegetation. This means when vegetation photosynthesizes, the ecosystem absorbs carbon from atmosphere (downward arrow) (Oliphant et al., 2018). RE is ecosystem respiration and as ecosystem respire it adds

carbon to the atmosphere (upward arrow). F_{CH_4} is methane emission that can be either released from soil and other organisms in the soil and add carbon to the atmosphere or be absorbed into soil (upward and downward arrow). F_G is carbon emission produced by livestock grazing through their respiration and digestion system and through methane released from their stomach to the atmosphere (upward arrow). Also, livestock manure can be absorbed into soil and ground water (downward arrow). Moreover, some of the carbon emission produced by livestock can be removed as they move away from meadow ecosystems (horizontal arrow). F_W is transported carbon as suspended or dissolve form through underground and surface water movement in the meadow ecosystem (upward and downward arrow).

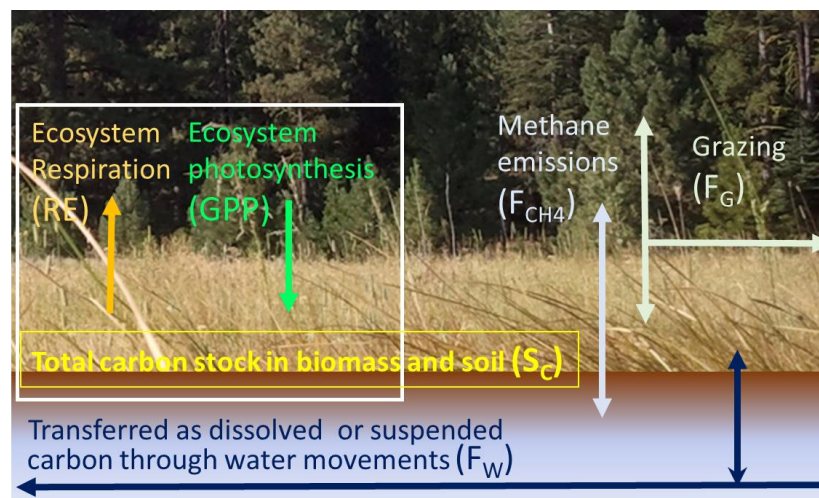


Figure 4: Conceptual model of major carbon movements in a meadow ecosystem (Adapted from: Oliphant et al., 2018)

1.7 Phenology of Sierra Nevada Meadows

In montane meadows plant phenology, the timing of plant life-cycle events, and seasonal productivity of hydric and mesic plant species depends on the availability of surface water and near surface ground water. The start of the growing season is largely governed by the timing of

snowpack melt on the meadow surface. Seasonal patterns in water and light availability drive phenologic shifts from plant growth to reproduction and senescence (Stucky et al., 2018). Sierra Nevada montane meadows have strong seasonality in a vegetation life cycle that starts with snowmelt in late spring. Snowmelt runoff will increase surface water and increase soil moisture and temperature that causes growth (emergent) in vegetation. Later in summer as the water table declines and soil moisture decreases, vegetation starts to senesce (Loheide & Gorelick 2007; Viers et al., 2013). Senescence period starts from August until winter dormancy. From November until April the meadow surface is frequently covered with snow, depending on the elevation and water year.

Regional climate change is altering the timing of plant phenological phases of the Sierra Nevada meadows as temperature and precipitation patterns change. With an increase of 1°C of air temperature in the winter it is likely that snowpack will decrease by 30% (Huning & AghaKouchak, 2018). This increase in temperature causes precipitation to fall increasingly as rain and less as snow. Therefore, this reduction in precipitation not only affects the water table and storage in meadows, but also causes spring melt to occur earlier. Based on Haunsaker et al. (2012), the timing of spring streamflow in Sierra Nevada meadows has shifted, with the peak of flow arriving three weeks earlier and decreases in the ratio of snow to rain.

1.8 Use of Phenological Observations to Characterize Carbon Cycling

Near-surface remote sensing and digital repeat photography (DRP) is becoming a frequently used tool to monitor vegetation phenology and has shown great promise for characterizing carbon fluxes for a range of ecosystems with different scales (Luo et al., 2018). In recent years, the PhenoCam network, which is a cooperative continental-scale phenological

observatory, by using near-surface remote sensing and high frequency DRP, is tracking vegetation phenology to provide continuous temporal coverage of phenological change of ecosystems in North America (Seyednasrollah, 2019). The phenology datasets provide information to aid scientists and land managers in anticipating the impacts of climate change or land use on terrestrial ecosystems (Seyednasrollah, 2019; Richardson et al., 2009). For example, Alberton et al. (2017) used digital photography to monitor plant phenology in southern Brazil in order to provide biological conservation plans. Vegetation phenology is sensitive to climate variability. Richardson et al. (2009) and Liu & Wu (2020), used DRP to monitor temporal variation of spring and fall phenology in temperate broadleaf forest, evergreen needleleaf forest, woody Savannas and wetlands ecosystems. Moreover, Toomey et al. (2015) showed that the green chromatic coordinate (GCC), vegetation greenness index, in a grassland increased during the growing season, photosynthetically active season, and remained high during summer when vegetation still had water available. Later in Fall, GCC decreased by 30% when vegetation senesced due to seasonality and decreasing access to water. Therefore, in grassland and meadow ecosystems, phenology responds strongly to the timing and magnitude of precipitation and seasonality (Toomey et al., 2015; Seyednasrollah, 2019; Richardson et al., 2009).

1.9 Research Objectives

There has been many studies and research on carbon fluxes in global ecosystems such as deciduous and coniferous forests, wetlands, and grasslands (Hirota et al., 2010; Baldocchi, 2008; Knox et al., 2015). However, studies that focus on meadow ecosystems are few, even though meadow ecosystems tend to be effective at sequestering atmospheric carbon and storing it in organic soils. Moreover, meadows are one of the most altered ecosystems by land use and is

vulnerable to climate change (Viers et al., 2011). In recent years different funding and restoration programs helped to restore meadow ecosystems, however, studies which focus on the impact of restoration on meadows and year-to-year variability are rare. Therefore, there is a need to understand the range of carbon fluxes under different meadow types, levels of degradation and precipitation years. Modeling carbon fluxes based on DRP has yet to be attempted in meadows, yet there is a great opportunity in applying DRP, since meadow ecosystems change color significantly over the growing and senescence seasons, as with most grasslands.

The main goal of this study is to investigate the use of digital repeat photography to determine ecosystem functioning and carbon sequestration in montane meadows of the Sierra Nevada. Our objectives include:

- 1) Advancing our understanding of seasonal patterns of meadow ecosystem CO₂ exchanges from eddy covariance observations and image analysis of digital repeat photography.
- 2) Generating empirical models that estimate ecosystem CO₂ exchange using just digital repeat photography.

1.10 Rationale for the Research

This research can help enhance future developments in using DRP to build models that extend our understanding of temporal changes in vegetation of the different ecosystems. The technique that has frequently been used for observing and assessing carbon cycling and monitoring temporal patterns of vegetation in an ecosystem is the eddy covariance technique, which compared to using GCC to assess the phenology of productivity is a time-consuming, expensive, and labor-intensive method (Richardson et al., 2011). DRP offers an automated, high

frequency and resolution data collection approach that is cost-effective, easy to install, and reduces fieldwork (Seyednasrollah, 2019; Alberton et al., 2017; Richardson et al., 2011). One of the advantages of the low-cost and portability of DRP is that we can expand the coverage of observations in order to compare carbon uptake performance in a range of meadows to learn more about their potential of carbon uptake, and the role of climate change, land-use managements and restoration plans. Moreover, the DRP technique enables a continuous monitoring of vegetation in meadows before, during and after restoration and over a longer period. This has been critical to many restoration projects where post restoration monitoring has often been short, showing only the initial rapid success. However, how the restored landscape functions within the overall ecosystem long term is less well understood (Pope et al., 2015). Moreover, DRP technique can be used to determine the plant phenology (life cycle) and phenological transition dates, which indicate the seasonal changes and magnitude of ecosystem carbon cycling.

Study Site

2.1 Red Clover Valley Ranch Location, History and Land Degradation

Clover Valley Ranch (39.94411, -120.4506) is located on the northeastern side of Sierra Nevada at the headwater of the north fork of the Feather River at 1478 meters (4848 ft) in elevation (Weather Portola, 2020). It includes 1,233 hectares (3,047 acres) of ranch land occupying a large meadow in Plumas County in California (The Sierra Fund, 2018). The valley is a large alluvial meadow surrounded by mountain ranges and coniferous forest. Crossing through the meadow are Dixie Creek, Crocker Creek and Red Clover Creek, which are part of the Feather River watershed (Figure 5). Crocker Creek enters the ranch from the southeast and Dixie Creek from the north and combines to create Red Clover Creek to the south (Figure 5). Although most of the valley floor is privately owned, the surrounding areas and foothills are part of Plumas National Forest and managed by U.S. National Forest. The valley does not have any developed campground or buildings, but has area suitable for camping and recreation activities, fishing, gaming, timbering and grazing (Watershed Restoration on the Plumas National Forest, 2020).



Figure 5: Location of Red Clover Valley Ranch, creeks and flux tower. (Source: Google Earth)

Red Clover Valley prior to European arrival was inhabited by Mountain Maidu and Washoe Indians. In 1875 the large barn was built, and valley became ranch land that supported 85 cows. In 1880, the diversion of Dixie Creek and Red Clover Creek began. In 1920, a railroad was constructed in the valley to provide transportation for logging, mining and dairy products (Red Clover Valley Restoration Project, 2013). In 1940-50, following a federal program, aerial herbicide spraying was conducted, eliminating riparian willow. During the same period, more than three hundred California Golden beavers were removed (Ponce & Lindquist, 1990). Eliminating the willows and beavers, along with heavy grazing, timber extraction, mining and railroad development caused severe erosion of creeks, and channels incised down to 3 meters below the meadow elevation (The Sierra Fund, 2018). This erosion caused a large amount of sediment to be washed into the Feather River through meadow tributaries. The flooding and

associated gullying lowered the water table. Lowering the water table caused a shift from wet meadow species dominated by sedges and willows to a dry sagebrush meadow (Ponce & Lindquist, 1990).

2.2 Red Clover Valley Restoration Project and Management

The restoration plan of the Red Clover Creek, and the region around it, started in 1985 by installing loose rock check dams (Ponce & Lindquist, 1990). Check dams are small dams built across a channel to decrease the runoff velocity, reduced the gullying in the channel and allowing sediments rate to increase. In 2013, Clover Valley Ranch was granted a perpetual conservation easement, The Dixie Conservation Easement, from the Natural Resources Conservation Service (NRCS) for grazing rights (The Sierra Fund, 2018). This easement covers a total of 1,851 acres, including meadow and wetland. As part of the approval for this easement, a \$2.15 million fund was setup for Wetland Restoration Plan. The purpose of the restoration project is to maintain and enhance the overall habitat condition for the wildlife in the wetlands and meadows of Red Clover Valley. As part of this easement, a Grazing Reserved Rights Pilot program was approved for using livestock as a tool for maintaining and enhancing the overall habitat conditions of the wetland and meadow (Clover Valley Ranch, 2017). Based on this easement livestock grazing conducting from July to October under NRCS Grazing Management (The Sierra Fund, 2018).

Additionally, in 2016 the California Department of Fish and Wildlife (CDFW), as part of the Greenhouse Gas Reduction Grant Projects, awarded \$680,974 to The Sierra Fund (TSF) for Restoration of the Red Clover Valley Ranch. The goal for this project is to improve the climate resilience of the ecosystem and community in Red Clover Valley. This includes reestablishment of hydrologic function, mesic vegetation and ecosystem resiliency by constructing of grade

control structures, beaver dam analogues (BDA) and revegetation of native grass and willows (The Sierra Fund, 2018). Moreover, Natural Resource Conservation Service (NRCS), Wetland Conservation program installed a series of grade control structures to slow the water passage through the meadow (The Sierra Fund, 2018). These activities attempt to bring environmental, economic and greenhouse gas sequestration benefits for species and people of the region, including Mountain Maidu Tribe (The Sierra Fund, 2018). Data from before and after restoration will be collected to indicate benefits of the restoration also help to set Best Management Practices (BMP) which are a combination of practices determined to be effective by university scientists, and involvement of Mountain Maidu tribe and Sierra Meadows Partnership (Clover Valley Ranch, 2017).

2.3 Red Clover Valley Climate, Location of Towers and Study Time

Red Clover Valley has a mountain Mediterranean climate with warm and dry summers and cold and wet winters. Based on Portola climate data, a rural community approximately 22 km to the southwest of Red Clover Valley and 153m lower than Red Clover Valley, the monthly mean temperature varies between -7 °C in January to 28 °C in July, and the annual mean precipitation is 591 mm (Weather Regional Climate Center, 2020). The warm, dry season is from June to September and cold season is from November to March (Figure 6) (Weather Regional Climate Center, 2020). However, afternoon thunderstorms can occur during the dry season. The wet season is from October to May with peak of snow in February and the lowest amount of precipitation in August. Precipitation varies interannually which impacts the volume and timing of the runoff and vegetation growth. Based on Grizzly Ridge, snow sensor site, approximately 22 km to the west of Red Clover Valley and 620 m higher in elevation, the 2019 water year was

44% above the 30-year average (median 2060 mm) with snowfall of 4180 mm from December till June. However, the 2020-21 water year was 60% lower than the 30-year average, with snow fall of 1450 mm from November till April (Natural Resources Conservation Service, 2021).

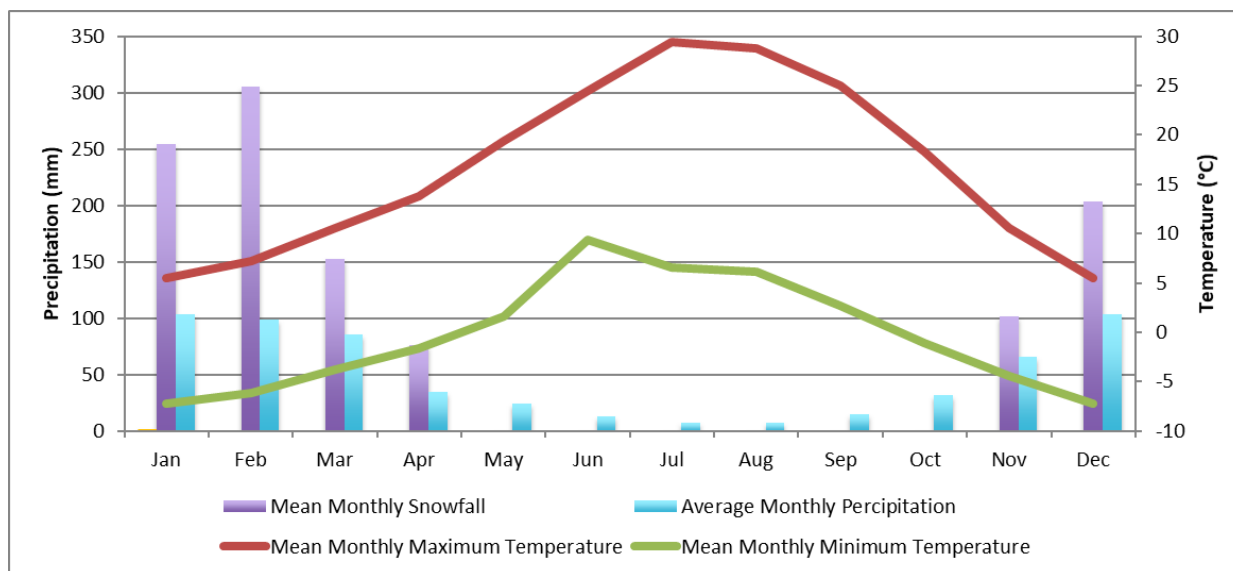


Figure 6: Climatology of study area. Thirty year (1981-2010) monthly average precipitation and monthly average minimum and maximum temperature for Portola, California. (Source: National Climate Data Center, NCDC).

Seasonality of Red Clover Valley vegetation can be identified from field observation and camera images. The growth season, emergent phase, starts in May, immediately after the snow melts. At this time, the meadow is saturated with water and the soil is warm, which supports the emergence of meadow plant species. Ecosystem leaf area index (LAI) and biomass rapidly increases towards the peak of the growing season in June or July. At this time vegetation reaches its maximum LAI and height; this is the beginning of the flowering period, followed by a long gradual senescence. From July/August, the vegetation height declines, and vegetation senescence occurs (senescence phase) (Figure 7). From late November till March the meadow vegetation

remains fairly dormant and may be covered with snow; however, the timing of snow season may vary from year to year.



Figure 7: Vegetation peak of growing season and senescence phase in Red Clover valley, 2019.

Our study in Red Clover Valley was conducted over three years. The first observation period was from June 02 to October 24, 2019 (RCV1). The second-year observations ran from August 08 to December 2020 (RCV2-2020) and the third year was from January to October 2021 (RCV2-2021). However, the Red Clover Valley meadow study will continue until 2023. Our first-year eddy covariance tower (RCV1) was located on the northeast of the meadow in a degraded area, dominated by mesic and xeric vegetation and our second-year eddy covariance tower (RCV2) was located near the center of the meadow in an area impacted by restoration and is dominated by mesic and hydric vegetation (Figure 5).

Methodology

To understand the seasonal pattern of carbon cycling and green chromatic coordinate (GCC) in Red Clover Valley and Loney Meadow as well as to generate empirical models based on DRP and carbon fluxes we used two different methods and instrumental design. In this section, we will first describe our use of DRP to derive a time series of meadow GCC and

describe our experimental design for DRP. Second, we will describe our use of the eddy covariance technique to directly measure carbon fluxes and provide a reference for comparing GCC directly to the carbon cycle.

3.1 Digital Repeat Photography (DRP)

DRP of vegetation is a form of near surface remote sensing that uses imaging sensors to monitor spatial and temporal patterns of vegetation. Compared to satellite remote sensing, DRP provides data with higher temporal frequency (minutes and hours) and higher spatial resolution (range of meters). DRP is also more robust to variation in illumination conditions and is rarely obscured by clouds (Richardson et al., 2009). This technique can provide high quality optical data to verify changes in the ecosystem, such as vegetation growth, biomass stage, and even carbon sequestration. Digital cameras used for monitoring plant phenology, also called “PhenoCams,” allow us to observe and detect the plant phenological events by analyzing the color change of vegetation (red, blue and green) over the time (Alberton et al., 2017; Richardson et al., 2009). Moreover, it can be used for monitoring crops, and other managed ecosystems, as well as natural ecosystems, and when joined in community networks, provide continuous ecological monitoring at regional to continental scales (Richardson et al., 2009; Migliavacca et al., 2011; Alberton et al., 2017).

Cameras that have been used for calculating GCC using DRP include commercial webcams from a range of manufacturers (Table 2). Based on the PhenoCam network, cameras are classified into three classes. Type I cameras follow standard protocols and actively engage as PhenoCam collaborators such as camera maintenance and troubleshooting; our camera in 2021 is a type I (Table 3). Type II cameras have some deviation from standards but are actively engaged.

Type III cameras deviate from standard protocols and do not actively engage as PhenoCam collaborators; our hunting camera in 2019, 2020 and 2021 is a type III (Table 3).

Table 2: Common model of camera used for digital repeat photography.

Camera model	Citation
Axis 211	Richardson et al., 2007
StarDot NetCam SC	Wharton et al., 2011; This study
Olympus D-360L	Yang et al., 2207
Canon VB-C10R	Sacks et al., 2007
Nikon Coolpix 990	Torn et al., 2010
D-Link DCS-900	Baldocchi et al., 2004
Campbell CC640	Migliavacca et al., 2011

3.2 Green Chromatic Coordinate (GCC)

From digital images we can calculate color indices, canopy green chromatic coordinate (GCC) which is an algebraic combinations of red, green and blue color channel (RGB) to encode brightness values or leaf color and investigate the phenological status of the vegetation (Migliavacca et al., 2011; Richardson et al., 2007; Alberton et al., 2017). Therefore, the vegetation phenological pattern (growth to senescence) can be described based on the proportion of green fraction in the image. Moreover, this temporal pattern and change in GCC can drive carbon exchange processes, such as photosynthesis and respiration (Migliavacca et al., 2011; Richardson et al., 2007; Alberton et al., 2017). For example, Toomey et al, 2015 used canopy greenness index to monitor the seasonality of gross primary production (GPP) of nine sites across the U.S. and found a strong relationship between canopy phenology and GPP. Similarly, Richardson et al., (2007) used GCC to understand the relationship between canopy structure and

the seasonal dynamics of photosynthetic uptake of CO₂ by forest canopy in Bartlett Forest in north central New Hampshire.

The color channel information of a digital image can be extracted as a separate digital number (DN) of red, green, blue (RGB). RGB DN are the average red, green and blue digital numbers that indicate intensity (Sonntag et al., 2012; Seyednasrollah et al., 2019). Since there is high correlation among the RGB color components, these color components need to be separated for quantitative analysis (Sonntag et al., 2012). Moreover, red, green and blue brightness levels are influenced by scene illumination. Therefore, this brightness should be separated by a nonlinear transform of RGB DN and then used for calculating the relative (normalized) brightness of each channel called RGB chromatic coordinate (RGB_{CC}) (Sonntag et al., 2012; Richardson et al., 2007; Alberton et al., 2017). The RGB_{CC} is a normalized (brightness) index (Equation 3), defined by dividing each component (channel DN) by the sum of all components (total DN) (Equation 2). Thus, GCC can be calculated based on Equation 4.

$$\text{Total RGB DN} = \text{Red DN} + \text{Green DN} + \text{Blue DN}, \text{ (Eq. 2)}$$

$$\text{chromatic coordinate} = \frac{\text{Channel DN}}{\text{Total RGB DN}}, \text{ (Eq. 3)}$$

$$\text{Green chromatic coordinate (GCC)} = \frac{\text{Green DN}}{\text{Total RGB DN}}, \text{ (Eq. 4)}$$

In addition to GCC, Excess Green (ExG) index also can apply in color time series analysis as:

$$\text{ExG} = 2G \text{ DN} - (R \text{ DN} + B \text{ DN}), \text{ (Eq. 5)}$$

This index can distinguish between green plants and their background, such as soil, by enhancing the signal from green plant material (Sonntag et al., 2012; Alberton et al., 2017).

Since ExG enhances the green signal of the plants, it can also be a useful tool for identifying healthy vegetation from diseased or damaged vegetation (Reid et al., 2016).

3.3 Digital Repeat Photography Experimental Design

For our first, second and third year of our study, (2019- 2021) in RCV1, RCV2-2020 and RCV2-2021 sites, we used a wildlife camera (Moultrie Inc.), and for our third year of our study, RCV2-2021, in 2021, we added a security/scientific camera (StarDot) that included an infrared (IR) filter (Table 3). Both cameras were installed on an eddy covariance tower at approximately 2.5 m height oriented towards the north. Both cameras were housed in weatherproof enclosures. The DRP data that we used for our study was only from the hunting camera.

The ideal height for installing the camera is 5 to 10 m above canopy. However, for shrublands and grasslands, the camera can be set up on a small tower close to the ground (1.5-3 m). Therefore, camera height may vary depending on the type of vegetation, nature of the tower, and the length of cables (Table 3) (Toomey et al., 2015; Richardson et al., 2009; Alberton et al., 2017). For an ideal field of view, the camera should point north (in the northern hemisphere) to minimize shadows, light interference from the sun, forward scatter, and lens flare. The incline should be up to 20° below horizontal and the field view of 60°. This means the camera should be adjusted to show 20% of sky and 80% of vegetation (Toomey et al., 2015; Richardson et al., 2007; Richardson et al., 2009).

To minimize the impact of day-to-day variations in scene illumination, especially when the sky is gray, the auto white balance (AWB) on the camera should be turned off and exposure adjustment should be set on custom, fixed white balance adjusting (R = 385, G = 256, B = 330) (Toomey et al., 2015; Seyednasrollah et al., 2019; The PHENOCAM network, 2018). White

balancing is adjusting digital numbers for each color channel in order to produce a neutral image for R, G, B values (Seyednasrollah et al., 2019). Therefore, AWB will affect the value of GCC, if the camera sets into AWB it will create an over estimation or “noise” of GCC values and hide the seasonality signal. This adjustment can be done by configuring the camera with PhenoCam Installation Tool (PIT).

Table 3: Camera type and specifications for each year of the study.

	Hunting camera	Security/Scientific camera
Model	Moultrie Inc., motion activated night vision	StarDot NetCam SC 5MP (CAM-SEC5IR-B)
Site	RCV1, RCV2-2020, RCV2-2021	RCV2-2021
Year of installation	2019, 2020 & 2021	2021
PhenoCam Type	III	I
Height of Camera installation (m)	≈ 2 for RCV1 & ≈ 2.5 for RCV2-2020 & RCV2-2021	≈ 2.5 for RCV-2021
Resolution	1920×1080 (full HD)	2592×1944
Power	four 1.5-volt C Cell batteries	12v battery
Data Storage	8 GB memory card	250 MB/ Data logger
Infrared Filter	No	Yes
Auto white/color balance	On	Off

Our cameras images were saved as 24-bit JPEG format (3840×2140-pixel resolution, with three channels of 8-bit standard RGB color information). The Moultrie camera took a picture six times each day with 60 minutes interval from 10:00 -15:00 hours. Our scientific camera took pictures from 4:00 to 20:00 hours with 30 minutes interval each day. We chose our interval because this will create high quality data sets and minimize data discontinuity in case of unfavorable weather conditions such as rain and snow; adverse illumination conditions due to

clouds or aerosols, and short-term power outages (Seyednasrollah et al., 2019). Moreover, bigger data sets reduce the impact of variation in day length over the course of seasons.

We collected 873 images for 2019 from our RCV1 site, 884 images for 2020 from our RCV2-2020 site; and 1632 images for 2021 from our RCV2-2021 site. To develop our GCC models we also included 120 images from Loney Meadow, located south of Yuba watershed in the Sierra Nevada, captured between May and September 2016 by a previous graduate student (Blackburn, 2017; Blackburn et al., 2021). To evaluate GCC as a predictor of photosynthesis and making empirical models, mean daily gross primary production (GPP) and net ecosystem production (NEP) values ($\text{gC m}^{-2} \text{d}^{-1}$) was regressed against average GCC values. We used linear, quadratic, and cubic regression.

3.4 Photo Quality Control

The first step for checking the quality of photos consists of searching for AWB errors in photos. As we are using a type III camera, Moultrie camera, and because this camera sets on AWB for removing the negative impacts of AWB on photos and data extracted, we used “grey world” AWB model proposed by Seyednasrollah et al. (2019).

$$\Delta = \left[\left(\frac{\overline{R_{DN}}}{\overline{R_{DN} + G_{DN} + B_{DN}}} - \frac{1}{3} \right)^2 + \left(\frac{\overline{G_{DN}}}{\overline{R_{DN} + G_{DN} + B_{DN}}} - \frac{1}{3} \right)^2 + \left(\frac{\overline{B_{DN}}}{\overline{R_{DN} + G_{DN} + B_{DN}}} - \frac{1}{3} \right)^2 \right]^{\frac{1}{2}}, \text{ (Eq. 6)}$$

Based on Equation 6, the average of red, blue and green digital numbers calculates across all the photos. If the grey world is smaller than, $\Delta < 0.02$, for more than 30 consecutive days then AWB error is suspected and data should be excluded because of poor quality (Seyednasrollah et al., 2019). All our photos for 2016, 2019 and 2020 passed this quality test and for year 2021 only winter days of year 23 till 60 had $\Delta < 0.02$, and this was during the presence of snow cover.

Another way to check the quality of photos is using a reference panel. A reference panel is a rectangular gray flat surface that can be installed in front of camera. Therefore, in the corner of every image there will be a gray panel during the whole study time (Figure 8). The reference panel is important to help monitor day-to-day shifts in color balance of the image that can occur due to changes in weather conditions and to evaluate long-term stability of the imaging sensor (The PHENOCAM network, 2018). Later, when processing the images, we calculate GCC for only reference panel. The GCC values of the reference panel for all the images varies day-to-day. However, over the seasonal timescale, changes in GCC values for the reference panel should be stable. If a change in the GCC is detected, the camera and reference panel should be carefully examined for degradation (The PHENOCAM network, 2018).



Figure 8: An example of a gray reference panel (red rectangle box), Red Clover Valley, August 2020.

3.5 Selecting the Region of Interest (ROI) and Data Processing

Image analysis is based on time series extracted from one to three specific regions of interest (ROI). Therefore, ROI can include a specific or several plant species, a population, a

portion of a canopy or a vegetation type in a heterogeneous landscape (Alberton et al., 2017). The dimension of the ROI was selected to provide a reasonably extended spatial sampling of vegetation while avoiding the inclusion of the area in the background that might be exposed to different light conditions or include other types of vegetation that we did not want to include in this study, such as conifer trees (Figure 9). Moreover, the size of the ROI has to be large enough to remove minor shifts in the field of view that can occur over time and can impact the chromatic coordinate values (The PHENOCAM network, 2018). For instance, for RCV1 we delineated three ROIs to sample each of the two plant communities, mesic and xeric in each photo (Figure 9).

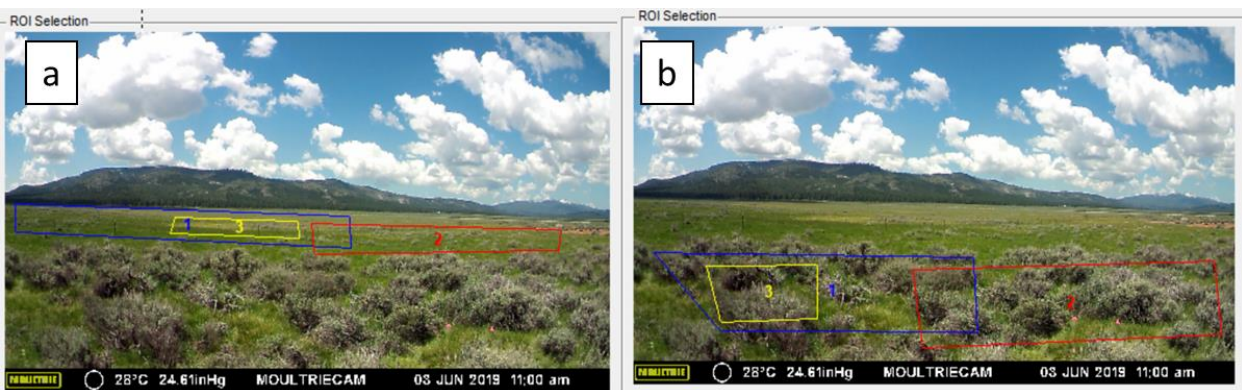


Figure 9: Example of selecting ROI for Red Clover Valley meadow, June 03, 2019, at 11:00. The blue, red and yellow ROIs selection (a) for mesic and (b) for xeric plant community to represent the sample to extract digital numbers.

Based on Equation 2, from each photo's ROIs, the red, blue and green DN values were extracted and then GCC calculated based on Equation 4. The software that we used for processing our images and calculating the GCC values is PhenoCam Image Processor (PCIP) also called PhenoCam GUI. PCIP is a stand-alone software built using MATLAB functionality (The PHENOCAM network, 2018).

Some of the images' quality were affected by light conditions, rain, snow, clouds, or even dirt on the camera housing. We did not do any selective editing or adjusting on these images. However, it is important while using PCIP software to calculate the 90th percentile value from all daily GCC values in a 3-day window (summary product) to minimize noise in the time-series information caused by illumination effects of seasonal changes, time of day and weather (Alberton et al., 2017; The PHENOCAM network, 2018). Moreover, if GCC values have outliers, the spline-based method can be used to remove them. In this method weighted scatterplot smoothing will be used to remove the outliers (Richardson et al., 2007; Seyednasrollah et al., 2019).

3.6 Eddy Covariance Technique and its Theory

The eddy covariance technique is a micrometeorological method for measurements of trace gas fluxes, as well as momentum and energy fluxes between the biosphere and atmosphere (Oliphant, 2012; Baldocchi, 2014). Estimating the trace gas fluxes is achieved through measuring the instantaneous covariance between upward and downward motions of air and the concentration of gases contained within the moving air parcels. The vertical component of turbulent eddies exchange gases between the surface and overlying atmosphere. The exchange of mass is calculated as:

$$F_s = \rho_a \overline{w's'} , \text{ (Eq. 7)}$$

where, the eddy flux of scalar (F_s) is the covariance between high frequency fluctuation in vertical wind velocity or wind speed (w') and scalar or fluctuations in the concentration of CO₂ and water vapor (gas) in the atmosphere (\bar{s}) multiplied by atmospheric density

(ρ_a) (Baldocchi, 2014; Oliphant, 2012). Therefore, by sampling the motions of the air at high speed for a long enough time, an average flux density of gas exchange (F_S) between a vegetated canopy and the atmosphere can be determined. The eddy flux, Equation 7, is based on Reynolds decomposition and elimination of some of its terms. This means this equation is simplified based on the assumption that atmospheric density and mean vertical flow are negligible over a homogenous surface (Burba, 2013).

3.7 Data Processing, Flux computation, Data correction and Rejection

The exchange of the gas and energy between the biosphere and atmosphere is rapid, therefore, the instruments need to take measurements at high frequency. This means that sampling frequency is 10 Hz and turbulent fluxes were calculated from 30-minute covariance averages from the 10 Hz data (Novick et al., 2013). For each averaging period, the time lag between the anemometer and gas analyzer was determined using a maximum covariance method (Xu & Baldocchi, 2004).

Eddy Flux Software and MATLAB were used for data processing and computing flux covariance from raw data. The first step is to remove any spikes. Spikes are exceeded values that happen as result of instrument error or disorderly physical environment (Blackburn, 2017; Xu & Baldocchi, 2004). The spikes should be removed from raw data before calculating 30-minute average covariances as spikes can affect up to 15% of flux measurements (Blackburn, 2017; Xu & Baldocchi, 2004; Burba, 2013). To remove spikes, the data will be rejected if it falls outside of an acceptable range (2.5 standard deviations). Moreover, we use planar fit (PF) coordinate rotations and Webb-Pearman-Leuning (WPL) corrections. PF rotation is needed to remove the scalar turbulent flux tilt error and also to correct vertical wind for misalignment of the sonic

anemometer with respect to the local wind streamlines. The WPL correction compensates for the fluctuation of air density driven by changes in temperature and water vapor affecting measured fluctuations of CO₂ and H₂O (Burba et al., 2013).

The second step after processing data (post-processing) is the “plausible limit test”. In this test we use a filter to exclude fluxes outside of the range of expected possible outcomes. For example, if the CO₂ concentration is outside of the range of 300-500 ppm they will be considered as implausible and will be rejected during the post-processing (Blackburn, 2017; Xu & Baldocchi, 2004). The third step is to use another filter to discard the data with a friction velocity lower than 0.2 ms⁻¹ ($U^* < 0.2 \text{ ms}^{-1}$) (Xu & Baldocchi, 2004). The insufficient turbulence by declining in the quality of the data causes an underestimation in the flux data. The low friction velocity mostly happens during the nighttime as wind during the nighttime are more stable than daytime winds during strong convective mixing (Blackburn, 2017).

3.8 CO₂ Flux Partitioning and Gap-Filling

The eddy covariance technique measures the net ecosystem production (NEP), which is a measure of the net exchange of carbon between an ecosystem and the atmosphere (per unit ground area) and is a primary value to determine if an ecosystem is a sink (+NEP) or source of carbon (-NEP) (Baldocchi, 2008; Oliphant, 2012). NEP consists of gross primary production (GPP), which is photosynthesis or carbon absorption by vegetation, and ecosystem respiration (RE), which is respiration done by heterotrophic and autotrophic organisms (Hirota et al., 2010). Therefore, ecosystem exchange (NEP) can be calculated as:

$$NEP = GPP - RE, \text{ (Eq. 8)}$$

Using the eddy covariance technique, nighttime values can be defined as RE, since there is no light available for photosynthesis (Baldocchi, 2008; Oliphant, 2012; Wohlfahrt et al, 2008). Empirical models for RE are derived based on the relationship between nocturnal NEP and soil moisture and temperature (Equation 9).

$$RE = b_0 \exp(bT_{soil}), \text{ (Eq. 9)}$$

These modeled RE values are used to gap-fill Re for daytime periods as well as missing nocturnal periods. During the daytime, measured values can be defined as NEP. Using these values and the gap-filled RE values, GPP can be calculated as:

$$GPP = NEP + RE, \text{ (Eq. 10)}$$

At night GPP can be assumed to be zero, and to replace missing daytime eddy covariance values, a light-use efficiency model is derived (Xu & Baldocchi, 2004). This typically uses a rectangular hyperbola fit to the relationship between good quality GPP observations and photosynthetically active radiation (PAR) (Equation 11).

$$GPP = \frac{\alpha \times A_{max} \times PAR}{A_{max} + \alpha \times PAR}, \text{ (Eq. 11)}$$

The eddy covariance (EC) system may experience malfunctioning instruments, power failure and bad weather conditions, which can all result in missing data values. Missing or rejected data are gap-filled using the modeled RE and GPP values described above.

3.10 Eddy Covariance Experimental Design

For this study we installed two eddy covariance towers, one in 2019 (RCV1) and one in 2020 (RCV2-2020 and RCV2-2021) in our study site (Figure 5). Based on Table 4, the height of

each tower varies. The height of tower depends on the height of vegetation, usually at twice the height of the vegetation (Xu & Baldocchi, 2004; Verma et al. 1989).

All towers consisted of a 3-D sonic anemometer, to measure wind speed in the three orthogonal directions, a fast response open path gas analyzer to measure gas concentration such as water vapor, CO₂ or CH₄ (Figure 10). The 3-D sonic anemometer and gas analyzer were wired into the SmartFlux data logger (Table 4). We also used a thermistor and hygistor, connected into a data logger, to measure air temperature and relative humidity (Table 5). Deep cycle 12 v batteries connected to solar panels supplies the power for all instruments (Table 4). For the tower including the SmartFlux, the raw 10Hz files were stored on the SmartFlux memory and 30 minutes averaged data were collected in a SmartFlux 16 GB flash drive; data for two other towers was stored on the data logger including a 16 GB SanDisk memory card (Table 4). The pyranometer and pyrgeometer were mounted on each tower to measure short and long wave radiometers and faced south to avoid the shadow of the tower and other instruments (Table 5). We mounted another radiometer to measure PAR, solar radiation between 400-700nm that is used for vegetation photosynthesis (Table 5). All the radiometers were connected to data logger. Heat flux plates, thermocouples, and soil moisture probe (Table 5) were buried under ground, near tower, to measure ground heat flux, soil temperature and soil water content at different depth.

The gas analyzer and 3-D sonic anemometer were mounted towards the north so that wind from West and East were not influenced by the tower and other instruments (Figure 10). The gas analyzer and 3-D sonic anemometer were mounted at different heights with different distances between them (Table 4). The small distance between the 3-D sonic anemometer and

gas analyzer would give us confidence that both gas analyzer and anemometer are measuring the same eddies.

Table 4: Comparison between eddy covariance towers

	RCV1 tower	RCV2 tower	Loney Meadow tower
Instrument Height (m)	2.9	3.4	2.44
Anemometer distance to gas analyzer (LI7500) (cm)	10	20	10
Anemometer distance to gas analyzer (LI7700) (cm)	No	35	No
Deep cycle 12v battery	2	6	2
Solar panel	1	4	1
Data processing and storage	Data logger	SmartFlux	Data logger

Table 5: List of instruments on the eddy covariance tower.

Name of Instrument	Instrument Type and Description	Units of Measurement
Thermistor/Hygistor	HMP45C Vaisala	°C / %
3-D Sonic Anemometer	3D CSAT3 Campbell Scientific Inc.	ms ⁻¹
Infrared Gas Analyzer (CO ₂ / H ₂ O)	IRGA, Li 7500, Li-Cor Inc., Lincoln, NE, USA	mgCm ⁻³ s ⁻¹ and gH ₂ O m ⁻³ s ⁻¹
Infrared Gas Analyzer (CH ₄)	IRGA, Li 77 00, Li-Cor Inc., Lincoln, NE, USA	mgCm ⁻³ s ⁻¹
Pyranometer and Pyrgeometer	NR01 HukseFlux	Wm ⁻²
PAR sensor	LI-190R	μmol s ⁻¹ m ⁻²
Heat flux plate	HFP01 HuskeFlux	Wm ⁻²
Ground thermocouples	E type: Omega	°C
Soil moisture probe	SoilVUE 10, Campbell Scientific Inc.	m ³ m ⁻³
Data logger	Campbell Scientific CR1000, CR 3000 and SmartFlux System Li-Cor Inc.	----
Memory card	ScanDisk-16 MB	----
Battery	Super Start Marine Deep Cycle. Recreational equipment battery	----
Solar Panel	100-Watt 12 Volt, Renogy	----
Tripod	-----	----



Figure 10: Eddy covariance tower with its instruments, installed at Red Clover Valley meadow, Ca, October 2020.

3.11 Eddy Covariance Tower Footprint

The eddy covariance tower measurement source area (flux footprint) depends on the wind direction, wind speed, atmospheric stability, surface roughness and height of tower (Novick et al., 2013). Flux footprint or fetch describes the cumulative normalized contribution to the flux from an upwind source area (Migliavacca et al., 2011). Therefore, the flux averaging period (30 minutes) variation in wind speed and direction produces an area of the surface that is represented in the flux average. As the distribution is approximately Gaussian, we can estimate the source area by using analytical models such as Hsieh et al., (2000) and by using on site measurements (Blackburn, 2017).

Based on Figure 11, our flux footprint for our RCV1 tower is represented by the 50th, 70th and 90th percentiles of flux source area measured around the tower over the 2019 growing season. The 70% of the fluxes measured are within 400 m flux footprint. In our site the

prevailing wind blew from the northeast during the night (mountain breeze) and the south and southwest during the day (valley breeze). This means that during the day the flux footprint is closer to the tower due to daytime instability in the surface layer. However, during the night as we have more stable atmosphere from northeast, the 90th percentile is further from the tower in that direction. By separating flux values by wind direction along a 120°-300° azimuth orientation, and as prevailing winds during the study were from the northeast and south directions, fluxes could be determined independently for two different plant communities: xeric dominated by sagebrush, and mesic dominated by grasses. This means that when wind blew from the north and northeast, fluxes were counted as xeric vegetation community; when wind blew from the south and southwest, fluxes were counted as mesic vegetation community (Figure 11).

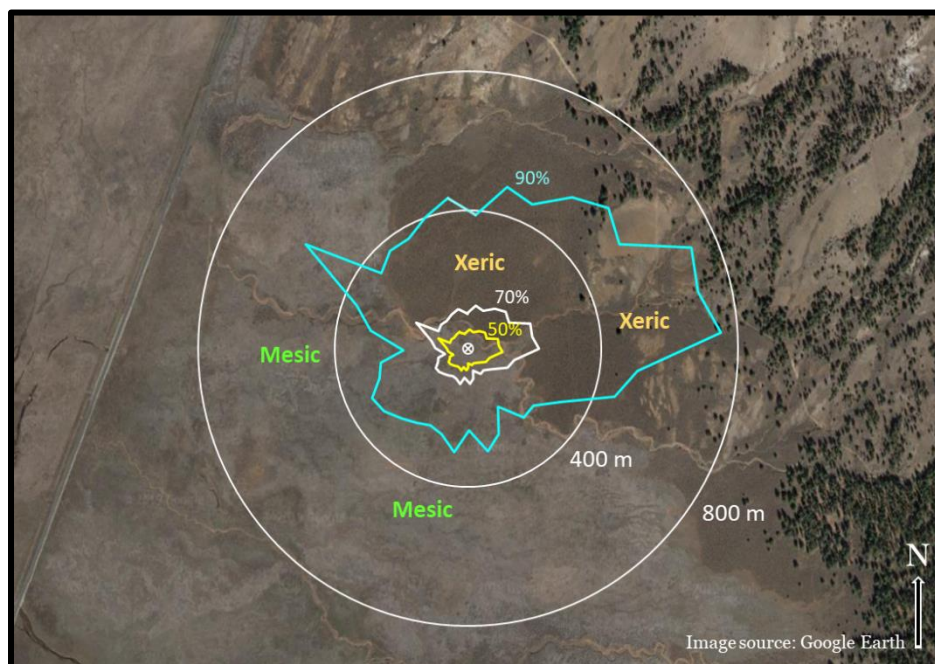


Figure 11: RCV1 flux tower footprint using the Hsieh (2000) analytical model, computed by MATLAB, located in Red Clover Valley, CA, 2019.

Results

4.1 Seasonal Patterns

4.1.1 Seasonal Patterns in Observed CO₂ Exchanges

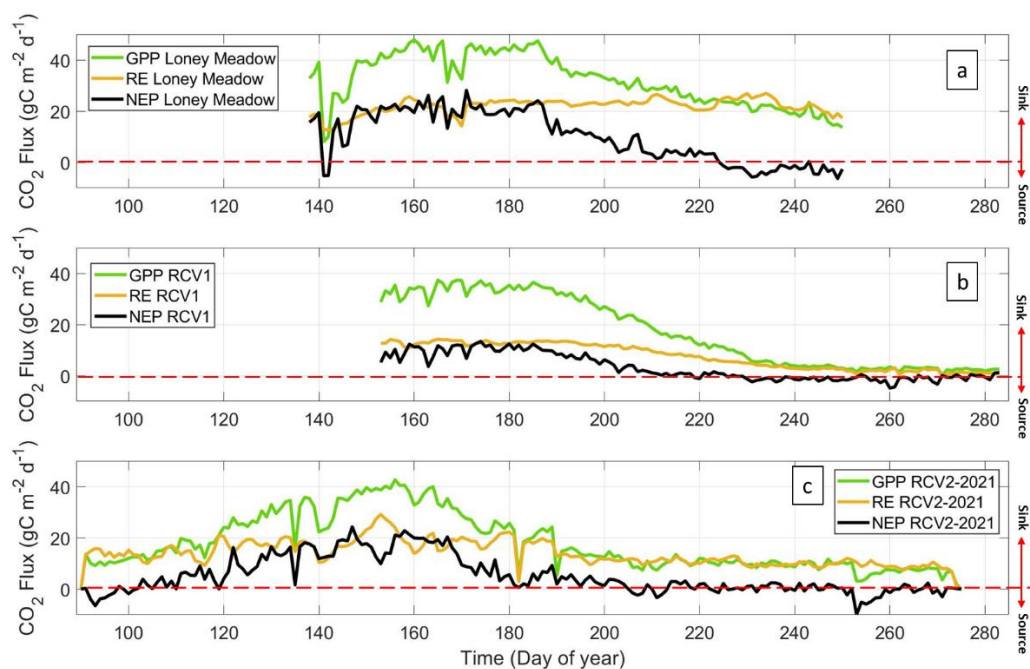


Figure 12: Seasonal pattern of gross primary production (GPP), respiration (RE), and net ecosystem production (NEP) in (a) Loney Meadow in 2016, (b) Red Clover Valley meadow (RCV1) in 2019 and (c) Red Clover Valley meadow (RCV2) in 2021 in the Sierra Nevada.

All three meadow-years assessed in this study showed similar seasonal patterns in CO₂ fluxes, despite different water years and meadows. Loney Meadow, RCV1 and RCV2-2021 were strong carbon sinks during the growth phase, with an average NEP of +18.46 gC m⁻²d⁻¹, +8.91 gC m⁻²d⁻¹ and +13.74 gC m⁻²d⁻¹, respectively (Figure 12). The growth phase for Loney Meadow and RCV1 was from the beginning of the observation record to July, approximately DOY 193 (Figure 12a and b) and for RCV2-2021 April, approximately DOY 119, to June approximately

DOY 178 (Figure 12c). Therefore, the growth phase for RCV2-2021 finished 15 days earlier than Loney Meadow and RCV1.

Based on Figure 12, RE was lower than GPP from the beginning of the observations until DOY 224 for Loney Meadow, DOY 237 for RCV1 and DOY 205 for RCV2-2021. However, after these days, RE exceeded GPP, resulting in Loney Meadow, RCV1, and RCV2-2021 to become weak sources of carbon during senescence phase, with an average NEP of $-2.03 \text{ gC m}^{-2}\text{d}^{-1}$, $-0.12 \text{ gC m}^{-2}\text{d}^{-1}$ and $-0.21 \text{ gC m}^{-2}\text{d}^{-1}$, respectively. All three meadows exhibited a long, slow senescence phase that led to a shift from a carbon sink to a carbon source. For Loney Meadow and RCV1 this shift occurred at nearly the same time (approximately DOY 224) and for RCV2-2021, it was three weeks earlier, approximately DOY 205 (Figure 12).

The peak of GPP for each meadow occurred at different times. In Loney Meadow it was on DOY 166, for RCV1 it was on DOY 174 and for RCV2-2021 it was on DOY 156 ($47.85 \text{ gC m}^{-2}\text{d}^{-1}$, $37.18 \text{ gC m}^{-2}\text{d}^{-1}$ and $42.66 \text{ gC m}^{-2}\text{d}^{-1}$, respectively) (Figure 12). Therefore, RCV2-2021 reached the peak of GPP 18 days earlier than RCV1 and 10 days earlier than Loney Meadow. Moreover, GPP in Loney Meadow and RCV2-2021 had larger day-to-day variability, especially in the first half of the growing season than RCV1. GPP for RCV2-2021 had a larger range ($24.51 \text{ gC m}^{-2}\text{d}^{-1}$) than Loney Meadow ($16.57 \text{ gC m}^{-2}\text{d}^{-1}$) and for RCV1, GPP mostly fluctuated around ($37.18\text{-}33.19 \text{ gC m}^{-2}\text{d}^{-1}$) during the growing season. GPP decreased more rapidly between DOY 200-220 for RCV1, however, for Loney Meadow after DOY 186 and RCV2-2021 after DOY 164, GPP decreased more gradually. This indicated that the senescence period for RCV1 was shorter than for Loney Meadow and for RCV2-2021 it was longer. Average GPP in Loney Meadow was 42% higher than RCV1 and 13% higher than RCV2-2021 during the growing

season. Similarly, average RE for Loney Meadow was 67% greater than RCV1 and 53% greater than RCV2-2021 during the senescence phase. Overall, Loney Meadow during the growing season became a greater carbon sink than RCV1 by 51% and RCV2-2021 by 25%. Although RCV1 received more precipitation than RCV2-2021, the meadow was in a more degraded condition at the RCV1 site, with a lower water table and different vegetation and RCV2-2021 was a larger sink of carbon during the growth phase.

4.1.2 Seasonal Patterns in GCC and RCC

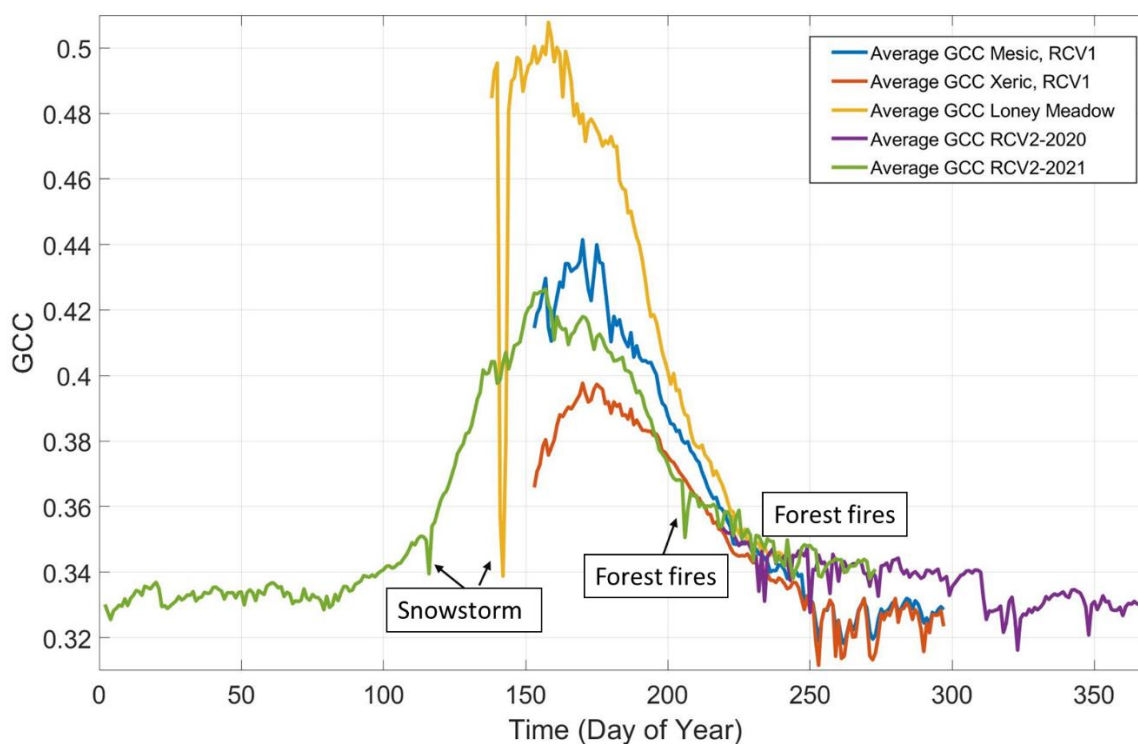


Figure 13: Seasonal pattern of green chromatic coordinate (GCC), of Loney Meadow in 2016, mesic and xeric communities of Red Clover Valley meadow (RCV1) in 2019 and RCV2 in 2020 and 2021.

Figure 13 shows phenological patterns throughout the different seasons using the green chromatic coordinate (GCC), detected by camera in different years in Loney Meadow, RCV1

and RCV2. Based on our site observations, Loney Meadow vegetation was mostly dominated by hydric vegetation community, RCV1 was dominated by mesic and xeric and RCV2-2020 and RCV2-2021 was dominated by mesic and hydric vegetation communities. GCC values started to increase during the growing season, DOY 138-156 for Loney Meadow, DOY 153-170 for RCV1-mesic and xeric and DOY 85-157 for RCV2-2021. However, for Loney Meadow and RCV1-mesic and xeric communities, the start of the growing season was significantly earlier than these DOY, as our measurement started during the growing season. As the growing season progressed, GCC reached its maximum values at the peak of growing season as follows: DOY 158 for Loney Meadow, DOY 170 for RCV1-mesic and xeric and DOY 157 for RCV2-2021 (Figure 13). Therefore, each meadow had a different growth phase duration with different timing of the peak of growing season. However, the growth phase for Loney Meadow and RCV2-2021 were closer to each other than RCV1. After this phase, GCC started to sharply decrease during the senescence phase for each meadow, DOY 159-236 for Loney Meadow, DOY 176-247 for RCV1-mesic and xeric and, DOY 156-240 for RCV2-2021. During the dormancy phase GCC values for RCV1-mesic and xeric, RCV2-2020 and RCV2-2021 had a gradual decline. GCC values for RCV2-2020 and RCV2-2021 during dormancy were almost the same magnitude. However, GCC values of RCV2-2020 and RCV2-2021 during the dormancy phase was higher than RCV1-mesic and xeric. RCV1, RCV2-2020 and RCV2-2021 reached dormancy almost at the same time (approximately DOY 245). RCV1-mesic and xeric reached dormancy (DOY 247) 7 days earlier than RCV2-2020 and RCV2-2021. Differences in GCC values occurred due to different locations, vegetation communities and meadow water availability (different water years).

The timing and duration of GCC values of each season differed between these three meadows and the GCC magnitudes were different as well (Figure 13). GCC for the mesic community in RCV1 during the peak of the growing phase was 6% lower than Loney meadow and GCC of the xeric community, during the same period, was 4% lower than the mesic community in RCV1 (Figure 13). GCC difference for the mesic community for RCV1 and RCV2-2021 was only about 2% during the peak of the growing season. However, we cannot see these differences in GCC throughout the whole growing season or senescence phase. As we get to the senescence phase, the difference in GCC values between the meadows and vegetation communities start to decrease. By the time that RCV1-mesic and xeric, RCV2-2020 and RCV2-2021 vegetation entered dormancy (approximately DOY 245), GCC converged on approximately 0.35 at the transition from the senescence to dormant phase. GCC values during dormancy for RCV2-2020 was higher than RCV1-mesic and xeric. There was a steep decline in GCC values for Loney Meadow (DOY 141) and RCV2-2021 (DOY 116) during a snow event. Snow on the ground lowered the GCC to 0.33 as fresh snow tended to scatter the three-color bands equally. However, the day after the snow event, GCC values increased sharply and immediately. The sharp dips in RCV1 and RCV2-2020 and RCV2-2021 during senescence phase and dormancy occurred during periods with high concentrations of wildfire smoke in the valley, which produced an orange sky color and lowered GCC values accordingly.

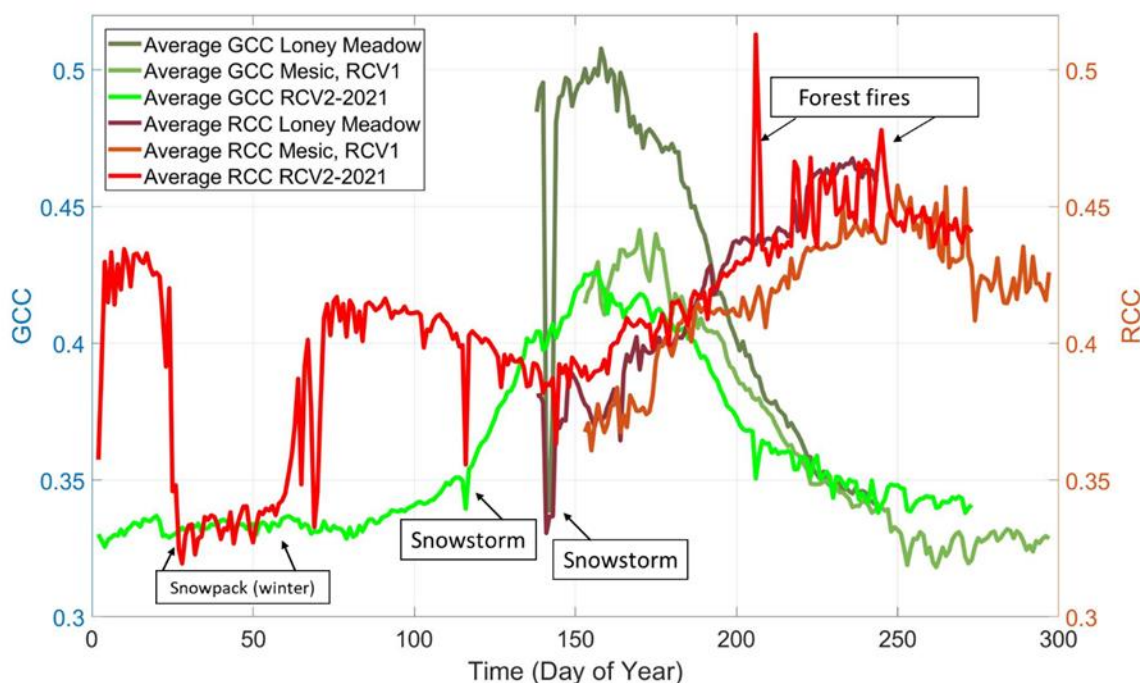


Figure 14: Seasonal patterns of green chromatic coordinate (GCC) and red chromatic coordinate (RCC), of Loney Meadow in 2016, mesic community of Red Clover Valley meadow (RCV1) in 2019 and (RCV2-2021) in 2021.

Figure 14 shows both GCC and the red chromatic coordinate (RCC) patterns for Loney Meadow, mesic vegetation community for RCV1 and RCV2-2021. Based on Figure 14, we can see that all three meadows became less green and more red as the growth season transitioned into the senescence period and then the dormancy phase. RCC patterns for the meadows were mostly opposite of GCC patterns, however, not completely. Because of this unlike GCC, RCC values during the growing season were lower than during the senescence phase. RCC during the peak of growing season for Loney meadow, RCV1 and RCV2-2021, had the minimum values (0.36, 0.37 and 0.36, respectively) and at the beginning of dormancy had the maximum values (0.46 and

0.45 and 0.46, respectively). Moreover, unlike GCC, differences in RCC values between meadows during the growth and senescence phase was less than 5%.

For RCV1 and RCV2-2021 the peak of RCC value was DOY 248 and 240 (respectively) which appears to indicate the end of the senescence period and the beginning of dormancy. Also, for Loney Meadow RCC reached its peak value on DOY 236, 11 days sooner than RCV1 and 4 days sooner than RCV2-2021. After that point, RCC values for Loney Meadow started to decrease however, due to the short data set, this decline was not clear (Figure 14). The upward spikes in the RCC values during the dormancy period were due to the local presence of regional wildfire smoke starting DOY 205 for RCV2-2021 (Figure 14). These corresponded with the dips in GCC values reported earlier. However, during snow events for Loney Meadow (DOY 141 and 142) and for RCV2-2021 (DOY 27 till 55 and 116) snow caused a decline in both RCC and GCC values to near 0.33. Therefore, it is possible to distinguish snow-cover, seasonal plant functioning and even the presence of wildfire smoke based only on the routine extraction of RCC and GCC values from repeat digital photography.

4.2 Relationship Between Seasonal Patterns of GCC, and CO₂ Exchanges

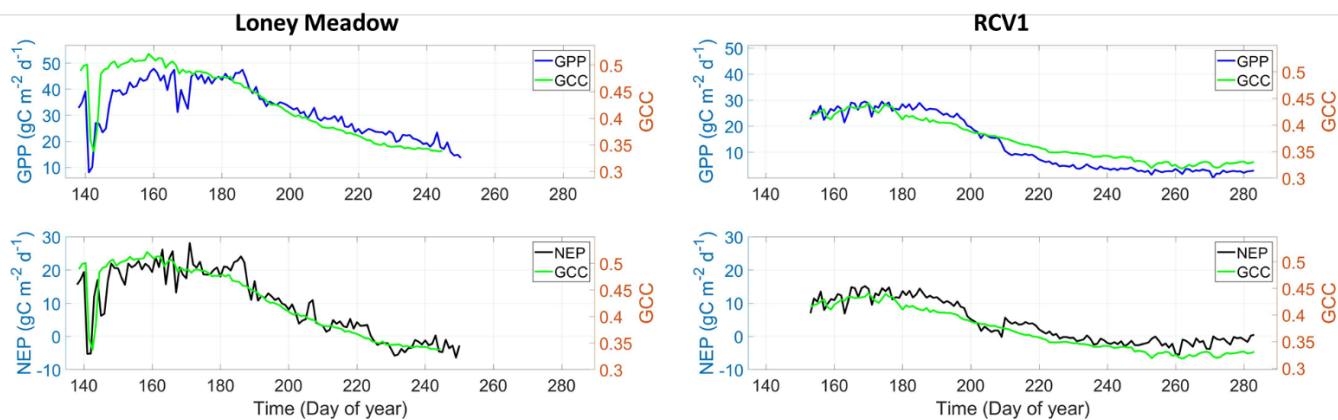


Figure 15: Seasonal patterns of (a) GCC and GPP, (b) GCC and NEP for Loney Meadow in 2016 and (c) GCC and GPP, (d) GCC and NEP for Red Clover Valley meadow (RCV1) in 2019.

GCC, GPP and NEP followed a similar seasonal pattern in Loney Meadow and RCV1 (Figure 15). Although the carbon fluxes are scaled differently to GCC, in Figure 15c, GPP relatively overestimated GCC values for the period immediately following the peak of the growing season and then after underestimated GCC values in the later senescence phase and dormancy for RCV1. We can also observe this overestimation and underestimation of GCC values by GPP for Loney Meadow (Figure 15a). However, the intensity of that was less than in the case of RCV1. GCC reached its peak values earlier than GPP, with Loney Meadow peaking 12 days earlier and RCV1, 4 days earlier. After reaching its peak values GCC started to decrease for both meadows, however, GPP remained high until 10-20 days after reaching its peak values and after that decreased rapidly for RCV1 (Figure 15c) and more gradually for Loney Meadow (Figure 15a).

From Figure 15b and d, it is evident that GCC had a closer relationship with NEP than GPP and this was more consistent over the growing season. Also, the timing of the GCC peak

and decrease in its values approximately match the NEP values. GCC values for both meadows had less day-to-day variability than GPP and NEP, especially during the senescence phase. This meant that plant reflection of green light was less sensitive to day-to-day weather variations such as clouds than the biophysical response indicated by GPP and NEP values.

4.3 Characterizing Seasonal Patterns in the Relationship with GCC, GPP and NEP

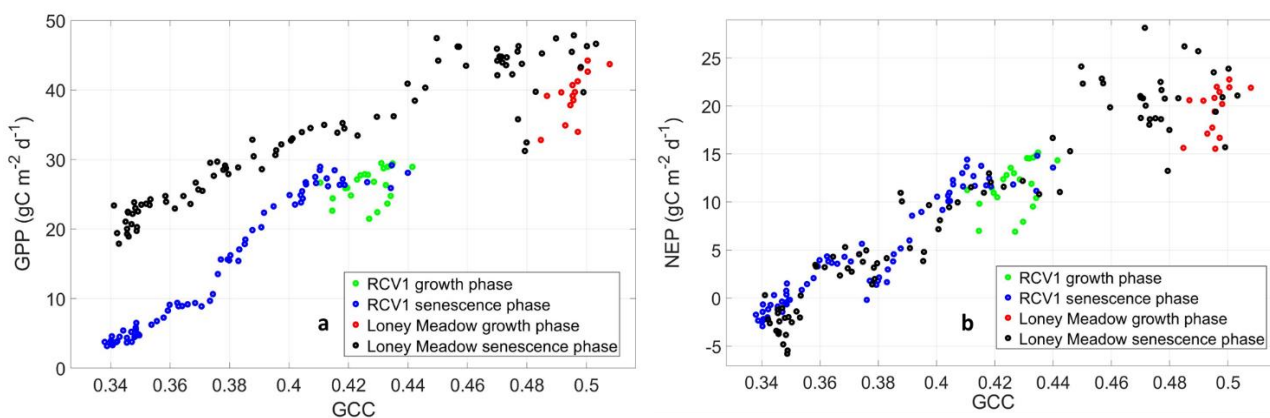


Figure 16: Growth phase and senescence phase for (a) daily GPP and GCC values and (b) NEP and GCC values for Loney Meadow, 2016, and Red Clover Valley meadow (RCV1), 2019.

In order to quantify the relationship between GCC and the two carbon flux terms, GPP and NEP, the carbon flux data were divided into the growth phase and senescence phase, separated by the peak of GCC values in the growing season. For Loney Meadow the peak of GCC was 0.51 and for RCV1 mesic community 0.44 (Figure 13). Therefore, the growth phase was from the beginning of data collection to the peak of GCC values for both meadows. The growth phase for Loney Meadow was DOY 138-158 (a duration of 20 days) and for RCV1 it was DOY 153-174 (a duration of 21 days). The senescence phase was defined as the period between the peak of GCC values and the beginning of vegetation dormancy when GCC had reached its peak value for both meadows (Figure 14). The senescence phase for Loney Meadow

occurred between DOY 159-244 (a duration of 85 days) and for RCV1 DOY 175-247 (a duration of 72 days). The reason for separation of phases, was to separate the phenological changes of vegetation based on meadow phenological pattern (phenophase). The growth phase characterizes the spring vegetation “green-up” and the senescence phase characterizes the autumnal senescence or “green-down” (Richardson et al., 2009; Zhou et al., 2020). Figure 16 shows the relationship between GCC and GPP (a) and GCC and NEP (b) separated into the two phases. In both meadows and both phases there was a positive linear relationship between the variables. However, the slopes and offsets of these linear trends were quite different between meadows and phases in the case of GPP (Figure 16a). For NEP, the differences between meadows and phases were much smaller, and it appeared that a single linear trend might describe them all equally well (Figure 16b).

4.4 Modeling GPP and NEP Using GCC

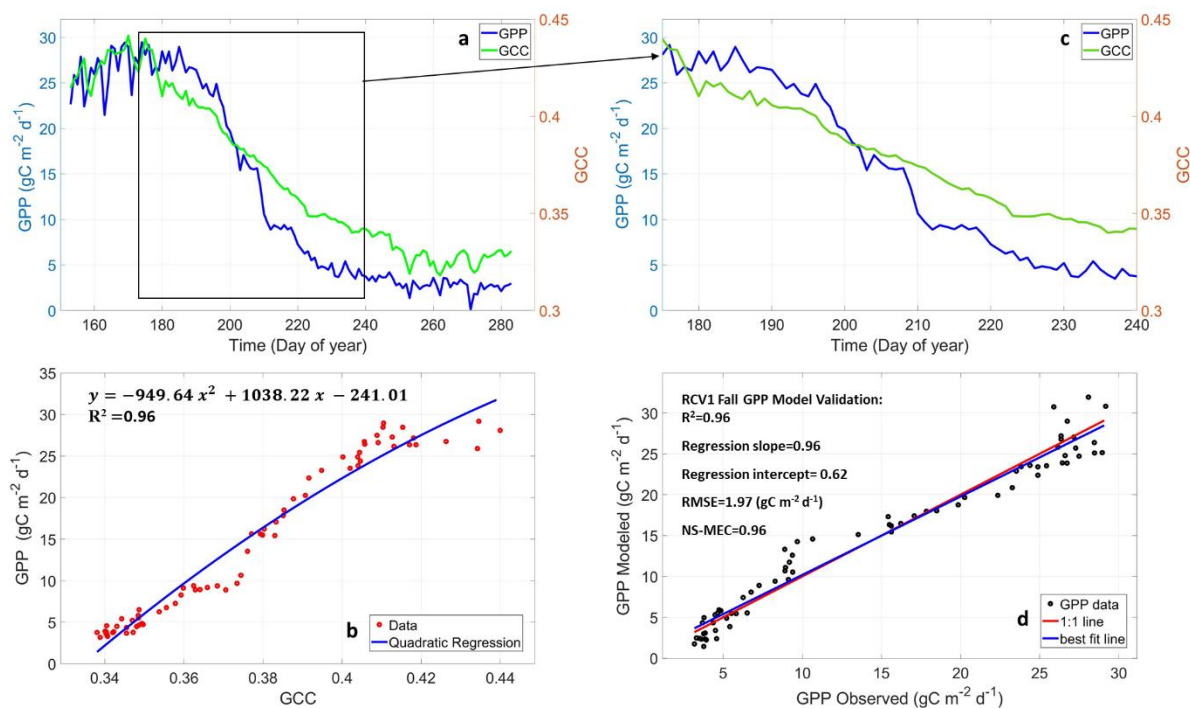


Figure 17: (a) seasonal pattern of GPP and GCC, (b) senescence phase pattern of GPP and GCC, (c) relationship between GPP and GCC, (d) accuracy graph of modeled GPP for Red Clover Valley meadow (RCV1), 2019.

Figure 17 is an example of how the overall process of creation of GPP and NEP models based on GCC values was conducted. In this example, after isolating data from the senescence phase (Figure 17a and b) and plotting GCC against GPP (Figure 16c), a positive correlation between GPP and GCC was produced. Then a quadratic regression equation was fit to the relationship, and an empirical model for GPP was derived (Equation 12).

$$\text{GPP} = -949.64 \text{GCC}^2 + 1038.22 \text{GCC} - 241.01, \text{ (Eq. 12)}$$

The slope of the equation represents that there was 1038.22 grams of carbon per square meter per day for every 1% increase in GCC. We tested the accuracy of our modeled GPP values, with GPP values that we observed with the EC tower (Figure 16d). Based on coefficient

of determination (R^2), and Nash Sutcliffe model efficiency coefficient (NS-MEC) this model can estimate the GPP values based on GCC for RCV1 senescence phase by 96% of validation (Figure 16d). Based on Figure 16c, the relationship between GPP and GCC, was not linear in the beginning and at the end of the senescence phase. This model underestimated GPP values in the end of the senescence phase and overestimated values in the beginning of senescence phase for RCV1. However, based on the NS-MEC value, which is the best fit around a 1-to-1 line, (0.96) this over and under estimation of GPP values are very small (only 4%).

4.4.1 Growth Phase Model

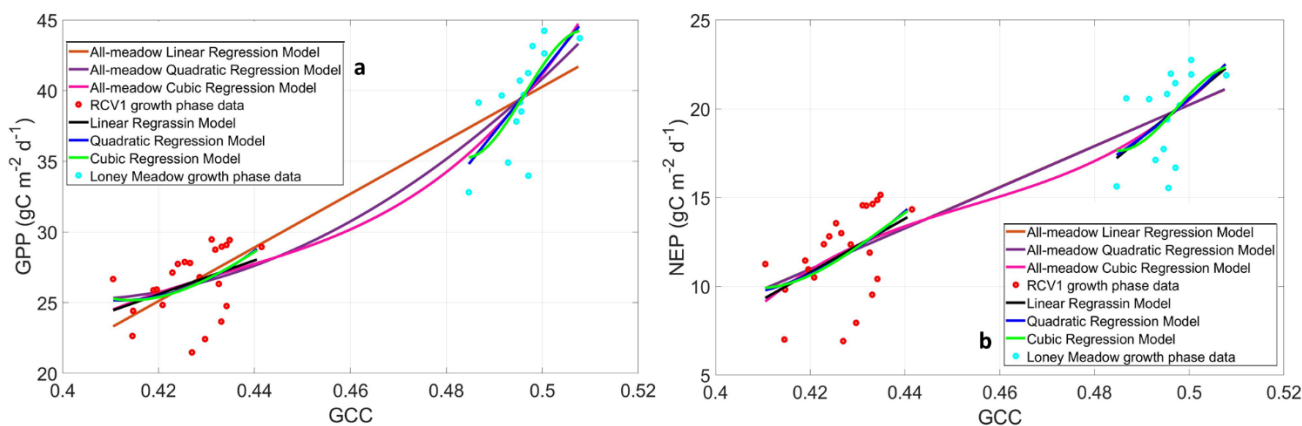


Figure 18: (a) GPP regression models based on GCC values (b) NEP regression models based on GCC values for Loney Meadow, 2016, Red Clover Valley meadow (RCV1), 2019, and all-meadows, for growth phase.

Figure 18 shows growth phase models of GPP and NEP based on GCC values. Based on Figure 18a, GPP and GCC are positively correlated during the growth phase. Both meadows had relatively small datasets in this phase, as we had less access to the meadows at the beginning of growth phase for measurements. Based on Figure 18a, the two datasets are very different, with Loney Meadow higher in both GCC and GPP than RCV1 during the growth phase. Loney

Meadow had a much narrower range of GCC (0.023) than RCV1 (0.032) during the growth phase. The reason is that Loney Meadow was dominated with hydric vegetation community and RCV1 with mesic community. Therefore, based on Figure 15, Loney Meadow's greenness increased rapidly and RCV1 greenness increased more gradually.

Best fit models were derived for both GPP and NEP, with GCC as the independent variable. These models were based on the relationship between GCC and GPP, NEP as evident in Figure 15. Although the relationships appear fairly linear, we explored three different regression models: linear, quadratic and cubic. For each regression model we derived an equation for the GPP and NEP, models, and coefficient of determination (R^2) value, and Nash-Sutcliffe model efficiency coefficient (NS-MEC) for validation of the model and root mean square deviation (RMSE) (Table 6 and 7). Based on Table 6, the validation of the GPP model for Loney Meadow was better than RCV1. Also, the regression slope of Loney Meadow is steeper than RCV1. This indicates that for RCV1, as GCC increased there was not much increase in GPP, especially earlier in growth phase when GCC was at its low values (0.41-0.42). This means the difference between rate of vegetation green-up and photosynthesis during vegetation growth season.

When both meadow's data are combined into an all-meadow model, the slopes for each meadow fall along a similar line (Figure 18a). The combined model greatly improved the goodness of fit relative to each individual meadow models. The quadratic fit connects the two individual meadow models best, although the R^2 is only 0.01 lower for a linear fit (Table 6).

Figure 18b shows the NEP growth phase model based on GCC values. NEP and GCC are positively correlated. Like GCC values in GPP modeling (Figure 18a), GCC values for Loney

Meadow and RCV1 in NEP modeling had a small range, causing low correlations, however, unlike GPP models, NEP models have approximately the same R^2 and NS-MEC values for both meadows (Table 6). When combining two meadows (Figure 18b) to create NEP all-meadow model, the fit was three times stronger using quadratic regression compared with the individual meadows (Table 6). This is presumably due to the much larger range in both variables, when combined.

Table 6: Regression equations and statistics for polynomial relationships between GCC and CO_2 fluxes for growth phase, where NS-MEC is the Nash-Sutcliffe model efficiency coefficient.

Site	Flux	Fit	Regression Equation	R^2	NS-MEC	RMSE	N
Loney Meadow	GPP	Linear	$y = 423.60 x - 170.50$	0.46	0.45	2.48	18
	GPP	Quadratic	$y = -5.11 x^2 + 428.67 x - 171.76$	0.46	0.46	2.47	18
	GPP	Cubic	$y = -1237023.87 x^3 + 1841854.83 x^2 - 913584.46 x + 150998.23$	0.46	0.46	2.45	18
	NEP	Linear	$y = 219.95 x - 89.38$	0.25	0.25	2.05	18
	NEP	Quadratic	$y = 2020.42 x^2 - 1782.65 x + 406.79$	0.25	0.25	2.05	18
	NEP	Cubic	$y = -673483.09 x^3 + 1004799.39 x^2 - 499406.35 x + 82709.52$	0.25	0.24	2.04	18
RCV1	GPP	Linear	$y = 119.75 x - 24.70$	0.15	0.15	2.17	21
	GPP	Quadratic	$y = 4416.28 x^2 - 3637.38 x + 774.12$	0.17	0.17	2.15	21
	GPP	Cubic	$y = -79870.75 x^3 + 106510.21 x^2 - 47126.52 x + 6947.59$	0.17	0.17	2.15	21
	NEP	Linear	$y = 151.55 x - 52.87$	0.22	0.22	2.16	21
	NEP	Quadratic	$y = 2704.86 x^2 - 2149.60 x + 436.39$	0.23	0.23	2.15	21
	NEP	Cubic	$y = -91922.02 x^3 + 120203.20 x^2 - 52200.58 x + 7541.34$	0.23	0.23	2.15	21
All-meadow	GPP	Linear	$y = 189.49 x - 54.47$	0.88	0.87	2.35	39
	GPP	Quadratic	$y = 1595.87 x^2 - 1279.54 x + 281.65$	0.89	0.89	2.34	39
	GPP	Cubic	$y = 25635.67 x^3 - 33349.07 x^2 + 14559.76 x - 2105.92$	0.89	0.89	2.31	39

Site	Flux	Fit	Regression Equation	R ²	NS-MEC	RMSE	N
	NEP	Linear	$y = 115.67 x - 37.62$	0.77	0.76	2.54	39
	NEP	Quadratic	$y = 14.46 x^2 + 102.35 x - 3457.78$	0.78	0.78	2.53	39
	NEP	Cubic	$y = 23328.61 x^3 - 31785.62x^2 + 14516.21 x - 2207.28$	0.89	0.89	2.12	39

Table 6 shows that by increasing the polynomial order, the validation of each model (R²) for Loney Meadow did not increase and for RCV1 it increased minimally (1-2%). For NEP the all-meadow model, using cubic regression caused an increase in model validation by 12%. However, this does not mean that cubic regression is the best model to define the shape of relationship between GPP or NEP and GCC. Moreover, based on Figure 15 and the positive correlation between GPP, NEP and GCC, we know that this correlation is not completely linear as GPP and NEP start to flatten at high GCC levels, which is the peak of the growing season. Therefore, we selected the quadratic regression for making our growth phase models as this model is the best representative to the shape of the relationship between GPP, NEP with GCC. In general, differences in the statistical confidence of the fit is negligible and a linear fit loses very little detail or accuracy.

4.4.2 Senescence Phase Model

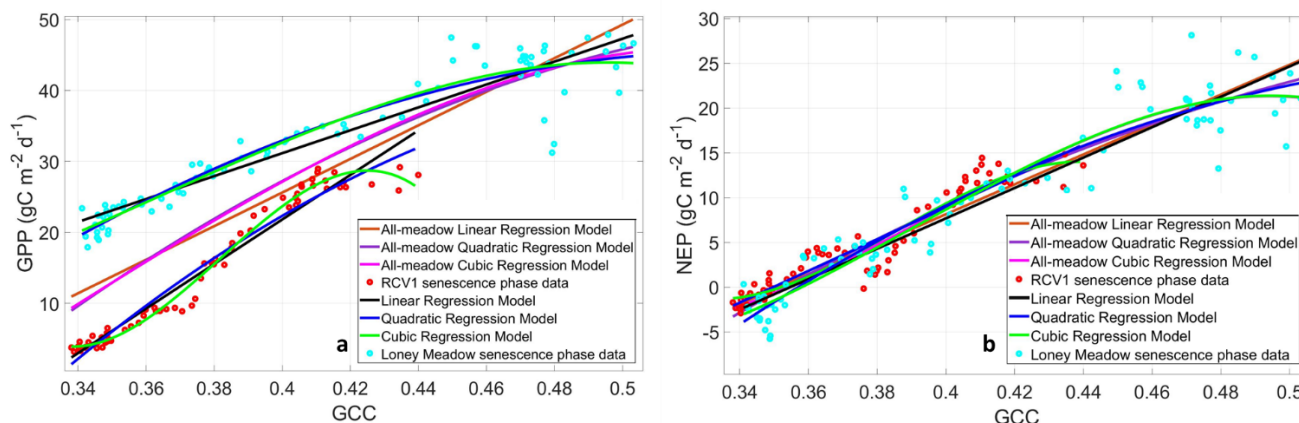


Figure 19: (a) GPP regression models based on GCC values, (b) NEP regression models based on GCC values for Loney Meadow, 2016, Red Clover Valley meadow (RCV1), 2019, and all-meadows, for senescence phase.

Figure 19 shows GPP models for Loney Meadow, RCV1 and all-meadows for senescence phase. Based on Figure 19a, GCC and GPP values during the senescence phase are highly positively correlated. Like GPP growth phase modeling, Loney Meadow in senescence phase modeling had higher GPP and GCC values. However, unlike GPP growth phase modeling, Loney Meadow had a wider range of GCC (0.16) than RCV1 (0.10). Also, unlike growth phase modeling, RCV1 had steeper slope value (31.37 of carbon per square meter for every 1% increase in GCC per day) than Loney Meadow (16.12 of carbon per square meter for every 1% increase in GCC per day) in linear regression (Table 7). This suggests that the rate at which GPP declined during the senescence phase was faster at RCV1 than Loney meadow. The reason was the distinctive seasonality difference between Loney Meadow and RCV1. Based on Figure 12a, GPP values for RCV1 at senescence phase decreased sharply and then flattened throughout the senescence period and resulted in RCV1 to have a very short senescence period. However, for

Loney Meadow, GPP values decreased gradually and therefore Loney Meadow had a longer and more sustained senescence period (Figure 12b). The GPP models for the RCV1 and Loney Meadow at the end of the senescence phase may underestimate the modeled values and overestimate at the beginning of the senescence phase. Figure 19a, includes the same regression modeled lines applied to both datasets to produce an all-meadow model, and the model equations and statistics are reported in Table 7. The quadratic regression model was still reasonable ($R^2=0.75$) despite different meadows and different water-years. However, the two populations are clearly different, and the model accuracy decreased markedly compared with the accuracy of each individual meadow-year.

Figure 19b shows NEP modeling for the senescence phase based on GCC values, using three different regression models. Also, it shows high positive correlation between NEP and GCC. Unlike NEP models for the growth phase (Figure 18b) NEP models for the senescence phase had a wider range. However, based on Figure 19b, Loney Meadow had a wider range (0.16) than RCV1(0.10). The slope of the linear regression for RCV1 ($176.7 \text{ gC m}^{-2} \text{ GCC}^{-1}$) is steeper than Loney Meadow ($169.6 \text{ gC m}^{-2} \text{ GCC}^{-1}$) (Table 7). This means that the RCV1 had a faster rate of decrease in NEP values than Loney Meadow during the senescence season. Moreover, the steeper slope of RCV1 model indicated that NEP was more sensitive to GCC than Loney Meadow (Figure 19b). However, overall Loney Meadow is greater carbon sink than RCV1 (Figure 12). Based on Figure 19b, both meadow's models underestimated NEP at high levels of GCC and overestimated NEP at low levels of GCC, and this is consistent between meadows. NEP for both meadows was almost the same magnitude, but this was not the case for GPP (Figure 19a) as Loney Meadow had higher GPP values than RCV1. The reason was that RE

was also higher for Loney Meadow than RCV1. Therefore, this led to a decrease in NEP for Loney Meadow lowering it to the level of RCV1's NEP. This means that based on Figure 19b, one model fits the relationship between NEP and GCC when we used data from two different meadows, with different vegetation communities and different sampling years.

Table 7: Regression equations and statistics for polynomial relationships between GCC and CO₂ fluxes for senescence phase, where NS-MEC is the Nash-Sutcliffe model efficiency coefficient.

Site	Flux	Fit	Regression Equation	R ²	NS-MEC	RMSE	N
Loney Meadow	GPP	Linear	$y = 161.28x - 33.36$	0.89	0.89	3.13	85
	GPP	Quadratic	$y = -673.58x^2 + 723.75x - 148.80$	0.91	0.91	2.82	85
	GPP	Cubic	$y = -4089.18x^3 + 4455.72x^2 - 1403.21x + 142.72$	0.91	0.91	2.80	85
	NEP	Linear	$y = 169.67x - 60.20$	0.91	0.91	2.94	85
	NEP	Quadratic	$y = -541.74x^2 + 622.05x - 153.04$	0.92	0.92	2.73	85
	NEP	Cubic	$y = -6601.99x^3 + 7739.53x^2 - 2811.94x + 317.63$	0.92	0.92	2.67	85
RCV1	GPP	Linear	$y = 313.72x - 103.51$	0.95	0.95	2.07	72
	GPP	Quadratic	$y = -949.64x^2 + 1038.22x - 241.01$	0.96	0.96	1.92	72
	GPP	Cubic	$y = -76281.38x^3 + 87364.58x^2 - 32923.35x + 4096.68$	0.96	0.96	1.11	72
	NEP	Linear	$y = 176.72x - 61.82$	0.90	0.90	1.78	72
	NEP	Quadratic	$y = -9.41x^2 + 183.90x - 63.18$	0.90	0.90	1.76	72
	NEP	Cubic	$y = -25776.38x^3 + 29833.01x^2 - 11292.11x + 1402.57$	0.91	0.91	1.68	72
All-meadow	GPP	Linear	$y = 236.55x - 69.01$	0.74	0.74	6.78	157
	GPP	Quadratic	$y = -671.96x^2 + 790.36x - 181.41$	0.75	0.75	6.54	157
	GPP	Cubic	$y = -2720.38x^3 + 2705.90x^2 - 595.68x + 6.56$	0.75	0.75	6.54	157
	NEP	Linear	$y = 166.97x - 58.66$	0.91	0.91	2.48	157
	NEP	Quadratic	$y = -367.3x^2 + 469.69x - 120.10$	0.92	0.92	2.41	157
	NEP	Cubic	$y = -7176.59x^3 + 8543.76x^2 - 3188.81x + 375.78$	0.92	0.92	2.34	157

Based on Table 7, the validation of models, R^2 , and NS-MEC values are higher for RCV1 than Loney Meadow (5-7%) for all three regression models. The main reason for the weaker fit at Loney Meadow was due to low outliers of GPP near the peak of the growing season. These are evident in Figure 15, and Blackburn et al. (2021) suggested it was due to a period of unsettled weather with unusual cloud cover and a large reduction in PAR at the daily timescale. For Loney Meadow the validation of GPP and NEP models for different regressions differ by only 1-2%. However, for RCV1, GPP models had higher validation by 5% than NEP models for all regression models (Table 7). For all-meadows modeling NEP models had higher validation than GPP models by 17%. The reason for this difference is that the magnitude of NEP for both meadows are the same, therefore, all-meadows NEP models have higher validation than all-meadows GPP models. Overall, based on Table 7, the difference between validation of linear, quadratic and cubic regressions is very small (0.01-0.02). This suggests that NEP, GPP and GCC relationships were almost linear. However, based on the shape of the data (Figure 19) and how data flattens at the beginning of the senescence phase for both meadows, quadratic regression still was the best method for modeling GPP and NEP during the senescence phase.

4.4.3 Combined All-Seasons Models

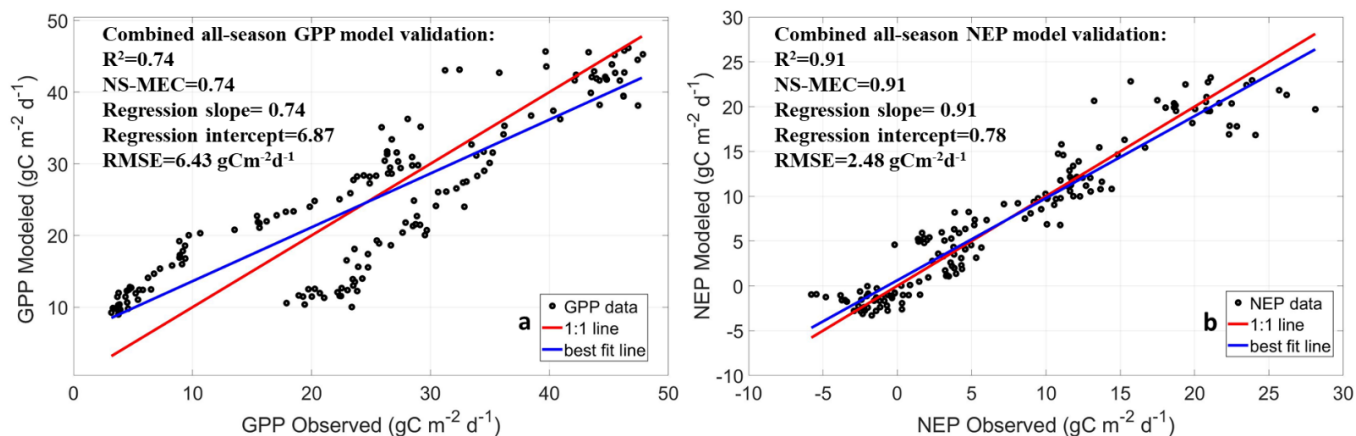


Figure 20: (a) combined all-seasons GPP modeled values accuracy and (b) combined all-seasons NEP modeled values accuracy, against observed carbon fluxes with eddy covariance for Loney Meadow, 2016, and Red Clover Valley meadow, RCV1, 2019.

Based on Figure 18 and 19, we modeled GPP and NEP for growth and senescence phase based on GCC values for Loney Meadow, RCV1 and all meadows together. Results from these figures and Figure 15 showed that the relationship between GPP, NEP and GCC is different in the growth and senescence phases as carbon fluxes, GCC, and phenological stages vary between meadows and between years. We also made models that did not separate meadows or phenological phases. In combined all-season models, all phenological phases data from two meadows combined in one model for GPP and one for NEP. Based on Figure 20, the modeled GPP and NEP are strongly and positively correlated with EC- observed GPP and NEP values. However, validation of NEP combined all-seasons model ($R^2=0.91$ and NS-MEC=0.91) is better than GPP combined all-seasons model ($R^2=0.74$ and NS-MEC=0.74). We observed the same results for all-meadow models for the senescence phase (Table 7) and opposite for all-meadows models for the growth phase (Table 6). Based on Figure 20a, and the difference between the best

fit line and 1to1 line, GPP combined all-seasons model underestimated values in the growing season and overestimated values during the meadows' senescence period. This was same for NEP combined all-seasons model (Figure 20b).

Discussion

The three meadow ecosystems studied in the Sierra Nevada functioned as a net sink (+NEP) of carbon during the main peak of the growing season (late spring/early summer) and a weak source (-NEP) of carbon starting in the late senescence period and continuing through the winter months. (Figure 12). Seasonal patterns in CO₂ fluxes in a low elevation grassland in California were also a moderate carbon sink during growth season and a weak carbon sink during the senescence period (Xu & Baldocchi 2004). Similarly, Knox et al., (2015) in a Californian wetland and Hiorta et al., (2012) in an Alpine meadow, found that carbon fluxes increased sharply during the emergent phase until the peak of the growing season (spring) and subsequently carbon fluxes decreased gradually as productivity of vegetation decreased during senescence phase. However, the exact timing of the growing season and the senescence period and duration of each season differed between each year and site. In the case of RCV2-2021 the carbon uptake period started from April with the peak of the growing season occurring in early June. However, based on Xu & Baldocchi (2004), carbon uptake period (sink) of a low elevation California grassland started very early (January) and reached its peak value in April. Moreover, based on Hirota et al. (2010), growth phase in Alpine meadow, in Qinghai-Tibetan plateau, started in April with peak of growing season in July. Our results indicated Loney Meadow and RCV1 started to become a weaker carbon source in August and RCV2-2021 in July (Figure 12).

Further, Xu & Baldocchi (2004), demonstrated that the low elevation California grassland had a very long carbon uptake period and started to become a weak carbon source in June. Our results showed that Loney Meadow and RCV1 compared with RCV2-2021 had a later start to become a carbon source (August). The reason is that Loney Meadow was a much wetter meadow at higher elevation on the west side of the Sierra Nevada Ridge. RCV1 at lower elevation on the eastern side of the Sierra Nevada happened in a record high year of precipitation and RCV2-2021 happened in a year of exceptionally low precipitation.

5.1 Water Availability and Vegetation Community Control on Carbon Exchange

Soil water availability is the major control on the growing season in meadow ecosystems, causing variations in NEP. The timing and intensity of precipitation as well as melt period are important factors, as these can impact NEP by changing the length of the growing season and the amount of RE (Blackburn et al., 2021). The timing of snow and timing of melt period drive the timing of soil water and how long snowmelt remains available through the summer. Especially during summer, rains enhance RE due to microbes becoming active in the surface soil layers. RCV2-2021 reached the peak of growing season 2-3 weeks earlier than RCV1 and Loney Meadow (Figure 12). The reason was that precipitation for RCV2-2021 started one month earlier (November) than RCV1 and Loney Meadow (December) (Natural Resources Conservation Service, 2021). Based on our results, Loney Meadow was a bigger sink of carbon than RCV1 and RCV2-2021 (Figure 12) as 2015-16 water year was 8% higher than 2018-19 water year (RCV1) and 78% higher than 2020-21(RCV2-2021) water year. Moreover, Reed et al. (2020) found that of the 13 Northern California montane meadows in their study, Loney Meadow was the wettest and most productive. As Loney Meadow is on the western crest of the Sierra Nevada

at higher elevation, it gets more precipitation, and more snow than RCV1 and RCV2-2021. Another explanation for variation in NEP between Loney Meadow, RCV1 and RCV2-2021 is that these meadows have different vegetation communities. The vegetation community of Loney Meadow was dominated by mixed graminoids and forbs, hydric to mesic vegetation communities (Blackburn et al., 2021). In 2016, Loney Meadow aboveground biomass was 150 g m⁻² (Reed et al., 2020). However, the RCV1 vegetation community was dominated by mesic communities in a degraded part of the meadow, with nearby channel incision evident. RCV2-2021 site was mostly dominated by mesic vegetation community (Table 1), but in a less disturbed part of the meadow, and an area impacted by upstream restoration efforts. The level of degradation at RCV1 was more severe than RCV2-2021 and Loney Meadow. Among these, Loney Meadow can hold the water for longer periods than RCV1 and RCV2-2021. Based on this, although the 2020-21 water year was 65% lower than the 2018-19 water year, differences in meadow vegetation communities and soil water ability caused RCV2-21 to become a slightly bigger sink of carbon than RCV1 (Figure 12).

Our results showed that Loney Meadow had higher GPP values than RCV1 and RCV2-2021 (Figure 12). The gradual decline in GPP in Loney Meadow suggests that the meadow was able to retain sub-surface water to sustain growth for a longer time slowing the rate of senescence. This is very important in carbon cycling in meadow ecosystems because when an ecosystem has a long senescence period, this will result in NEP staying positive, (a net CO₂ sink), continuing to accumulate the annual carbon sink. However, when we have an ecosystem with a shorter, steeper senescence period the transition between sink to source of carbon will happen earlier and thereby lower the annual carbon budget.

5.2 Separating Phenophases and Choosing Seasonal Phases

For estimating the phenological transition date (PTD) between the growth, and senescence phases, we selected the maximum GCC value like many other studies (e.g. Liu & Wu 2020). We found that the high values of GCC for each meadow and each year, almost corresponded and matched the high values of GPP and NEP (Figure 15). Moreover, for determining the end of senescence phase, based on maximum fall coloring, red, we used the date that maximum RCC value was detected (Figure 14) (Richardson et al., 2009; Toomey et al., 2015). RCC values clearly showed a second PTD at the end of the senescence phase and beginning of the dormant phase by the clear peak in RCC values. Hence, by combining GCC and RCC (Figure 14) we were able to find exact timings of different phases of the phenological cycle in montane meadows. Comparisons shown here reveal that each meadow and each year has a different timing for PTD. The PTD for Loney Meadow and RCV2-2021 was almost same date and for RCV1 was one week after Loney Meadow and RCV2-2021 (Figure 13). Therefore, this variation in rates of spring increase and fall decrease in daily GPP and GCC between years, caused that the dates corresponding to the start and end of the growing phase may not fully characterize the pattern of interannual variability in phenology (Richardson et al., 2010; Toomey et al., 2015).

Another way to estimate PTD is fitting GCC data to a sigmoid shaped logistic function (Toomey et al., 2015; Richardson et al., 2009; Fisher and Mustard, 2007). Therefore, the phenophase transitions are determined by calculating the minima and maxima in the curvature change rate of the sigmoid function. The maxima correspond to dates of the start of spring when vegetation leaf unfolding occurred, and the maximum greenness values represent the end of

spring and growth phase. The minima correspond to dates of end of senescence phase when leaf abscission occurs. This function also can estimate the midpoint of each phase (Toomey et al., 2015; Richardson et al., 2009).

5.3 GPP and GCC Relationship in Different Phenological Phases

Based on this study, GCC and GPP relationships in meadow ecosystems fluctuated seasonally. Our results (Figure 13) and other studies indicated, GCC had the highest values during the peak of growth phase and lowest values during the late senescence and dormant phase (Toomey et al., 2015; Zeri et al., 2011). Based on Figure 15, daily GPP increased more slowly throughout the spring, growth phase, and reached its maximum values 10-30 days after that GCC reached its peak for both meadows. This was also indicated in previous studies by Toomey et al., (2015), and Richardson et al., (2010), who concluded there was a 50–80-day difference between vegetation green-up and maximum vegetation photosynthesis. This means vegetation can reach the maximum green-up but not the leaf area index (LAI) or leaf chlorophyll content (Nagai et al., 2011; Keenan et al., 2012; Toomey et al., 2015). Similarly, our results showed that during the late growth phase and beginning of senescence phase GPP continued to increase and remain high for 10-20 days when vegetation green-down appears (Figure 15). Based on Figure 18a and Table 6, the correlation between GCC and GPP was weak in the growth phase, especially for RCV1. The healthy emerging spring vegetation produced high greenness values once it reached 100% cover early in the spring growth. Later, as the LAI and biomass continued to increase GCC increased by a small amount compared with GPP. In an alpine meadow site in Japan, GCC reached its peak 20-30 days after GPP peaked, indicating a significant lag time between peak greenness detected remotely and the actual carbon uptake by plants (Zhou et al. 2020).

In both meadows studied here (Table 6 and 7) and the Japanese alpine meadow (Zhou et al. 2020), growth phase models were statistically weaker compared with senescence phase models. One reason for this could be that we have fewer data for growth phase than senescence phase, because the growth phase (or the measurement period) was shorter. The late start to measurements in both meadow cases in this study means GCC was already quite high, and varied over the period by only a few percentages, while GPP changed considerably. Zhou et al. (2020), had a similar imbalance in data length. The mismatch in timing between peak GCC and peak GPP also confounds the statistics in the growth phase relationship between GCC and GPP. This was also found in the Japanese alpine meadow case (Zhou et al., 2020).

5.4 GPP vs. NEP Modeling

Digital repeat photography and GCC not only let us identify phenological patterns but helped to model day-to-day changes in the meadow carbon budget and variability in carbon cycling of the different ecosystems (Toomey et al., 2015). However, based on Figure 20, for modeling the carbon exchange in a meadow ecosystem in Northeastern Sierra Nevada, we may not need to separate the phenological phases because a quadratic regression model can estimate NEP or GPP for both growth and senescence phases. This can be investigated as longer datasets emerge in the future. We found that the correlation between NEP and GCC was higher than GPP and GCC for the combined all-season model (17% higher R^2), for all-meadow senescence phase model (17%) and RCV1 growth phase model (6%). However, this was the opposite for the RCV1 senescence phase model, which GPP/GCC correlation was (6%) higher than NEP/GCC. This was also the case for the Loney Meadow growth phase model (20%) and the all-meadows growth phase model (11%). Moreover, during the peak of the growing season, GPP for both

meadows overestimated GCC values and in the late growth phase and senescence period, GPP underestimated GCC values. However, this overestimation and underestimation is minimal for NEP. The relatively early peak in GCC relative to GPP as discussed earlier is less evident in NEP (Figure 15). This suggests that the high productivity rate following the GCC peak was compensated by similarly high RE rates, and this is borne out in the evidence (Figure 12). Secondly, the decline in GPP following its peak is much steeper than the decline in RE during the senescence phase. These differences combined produce a closer fit to NEP than GPP. A biophysical explanation could be that, although phenological patterns (and GCC) is an indicator of the amount of photosynthesis and is significantly correlated with GPP, plant phenology does not always correlate exactly with plant physiology (Liu and Wu, 2020). GCC is calculated based on a simple equation on visible bands, which covary to a significant degree with rates of ecosystem photosynthesis. Therefore, vegetation green-up can reach its maximum before the EC tower measures maximum GPP produced at physiological maturity.

Our study showed that quadratic regression models can estimate NEP and GPP with promising accuracy based on GCC values in different phenological phases for meadow ecosystems in the Sierra Nevada. Moreover, our results showed that NEP was more accurately predicted than GPP based on GCC, and that the model differences between meadows was much smaller. This means a universal model could be applied to both meadows with high accuracy. Previous studies have tended to estimate GPP and NEP by generating models for separate seasons, and there are few studies that model NEP and GPP based on GCC in a meadow ecosystem. Liu & Wu (2020) could not find any significant correlation between NEP and GCC for a broadleaf forest, evergreen needleleaf forest, woody Savannas and wetlands as NEP was

explained better with plant physiology than phenology. However, for grasslands they found the opposite, and phenology showed a better performance to describe NEP, as found in this study. The reason could be differences in vegetation type, particularly structural elements of vegetation, such as leaf area index, biomass, and canopy height, and environmental variables in different ecosystems. In grasslands and similarly in meadow ecosystems, the vegetation color changes significantly through the seasonal cycle (Figure 14) in response to change in seasons, particularly light, temperature and water availability. This suggests that, unlike other ecosystems, vegetation phenology and physiology are highly correlated in grasslands and meadow ecosystems. These modeling results are promising as a possible method to monitor carbon fluxes in mountain meadows. However, there is a need for more observational studies in meadow ecosystems that match direct measurement of carbon fluxes with phenological observations of GCC. This will more directly address why NEP models are more suitable than GPP models in meadow ecosystems. Moreover, our results suggested that phenological patterns and carbon fluxes need to be measured for longer durations to better understand inter-annual variability associated with climate. Additional studies will help to determine why relationships between GCC and NEP/GPP differ between meadows and years. This will hopefully allow for the development of universal models that can be applied across meadows within an eco-region.

Conclusion

Montane meadows of the Sierra Nevada contain complex ecosystems that respond to changing hydroclimate and geomorphic conditions that impact water table depth. Meadow ecosystems in the northern Sierra Nevada include components of xeric (sagebrush), mesic (grass

and forb) and hydric (sedge and rush) plant communities. The most important driver of productivity in a meadow is availability of near-surface water throughout the growing season. Meadow plant phenology similarly responds to changes in soil water availability. Anthropogenic activities and land use over the years have altered these ecosystems, generally resulting in meadows losing resiliency and becoming even more vulnerable to regional climate change. Restoration projects have helped to restore meadow hydrology in the Sierra Nevada. However, there are few observations of meadow carbon cycling, particularly variability associated with different hydroclimate years or the impact of meadow degradation and restoration. In this study, we used eddy covariance observations of CO₂ fluxes in three meadows combined with spectral information from digital repeat photography (DRP). We generated empirical models that estimated CO₂ exchanges based on the green chromatic coordinate calculated from DRP for meadow vegetation on a daily basis.

Our results show that all three meadows were strong carbon sinks during the growth phase and exhibited a long, slow senescence phase that led to a shift from a carbon sink to a carbon source (approximately DOY 224 for Loney Meadow and RCV1 and DOY 205 for RCV2-2021 dates). Soil water availability was found to be the main driver of carbon fluxes over the growing season. Therefore, Loney Meadow was a bigger sink of carbon than RCV1 and RCV2-2021 as 2015-16 water year was higher than 2018-19 and 2020-21 water year. Moreover, the variation in NEP between Loney Meadow, RCV1 and RCV2-2021 is due to different vegetation communities as the level of degradation of each meadow was different. The level of degradation at RCV1 was more severe than RCV2-2021 and Loney Meadow. As a result, Loney Meadow was able to hold the water for longer periods than RCV1 or RCV2-2021.

Our results indicate GCC values started to increase during spring months and reached its maximum values at the peak of growing season. During the senescence phase GCC started to sharply decrease for all meadows, however, during the dormancy GCC values had a gradual decline. GCC values for each meadow and each vegetation community and measurement year was different. The reason for this difference was due to difference in vegetation communities, elevation and meadow water availability. RCC patterns for the meadows mostly mirrored patterns of GCC, except when the meadow was snow covered, in which case the magnitudes converged.

There was a close relationship between GCC and both GPP and NEP, and this relationship was found to be best described by a quadratic regression which is used to model the carbon flux based on GCC. This relationship was different (and therefore modeled separately) for the growth and senescence phases. In general, model validation showed promising accuracy for both carbon fluxes. However, the NEP model performed more accurately than the GPP model. This is likely due to RE rates that scale with, and therefore partly compensate, GPP rates, reducing the range in flux magnitudes. This results in NEP being a better fit to GCC than GPP, a conclusion drawn in studies of other grasslands but not in forested ecosystems. The correlation between GCC and GPP was also found to be weaker in the growth phase than the senescence due, in part to a delay between plant phenological changes and associated physiological response, and a smaller sample size during the growth phase.

DRP and GCC enable us to identify phenological patterns and help to model day-to-day changes in the meadow carbon budget and variability in carbon cycling. By expanding DRP and GPP/NEP modeling and using GCC in meadow ecosystems, through comparing carbon uptake

performance, we can expand the coverage of observations with the use of low-cost portable digital cameras. This will expand our understanding of the potential for atmospheric carbon uptake, and the role of climate change, land-use management, and meadow restoration plans. Further, the use of DRP technique enables a continuous monitoring of vegetation in meadows before, during and after restoration and over a longer period, critical for understanding the complex dynamics of meadow ecosystems.

References

- Alberton, B., Torres, R. D., Cancian, L. F., Borges, B. D., Almeida, J., Mariano, G. C., . . . Morellato, L. P. (2017). Introducing digital cameras to monitor plant phenology in the tropics: Applications for conservation. *Perspectives in Ecology and Conservation*, 15(2), 82-90. doi:10.1016/j.pecon.2017.06.004
- Allen-Diaz, B. (1991). Water table and plant species relationships in Sierra Nevada meadows. *American Midland Naturalist* 126:30-43.
- Badiou, P., R. McDougal, D. Pennock and B. Clark. (2011). Greenhouse gas emissions and carbon sequestration potential in restored wetlands of the Canadian prairie pothole region. *Wetlands Ecology and Management* 19:237–256
- Baldocchi, D. D., Xu, L., & Kiang, N. (2004). How plant functional-type, weather, seasonal drought, and soil physical properties alter water and energy fluxes of an oak–grass savanna and an annual grassland. *Agricultural and Forest Meteorology*, 123(1-2), 13–39. <https://doi.org/10.1016/j.agrformet.2003.11.006>
- Baldocchi, D. (2008). Breathing of the terrestrial biosphere: lessons learned from a global network of carbon dioxide flux measurement systems. *Australian Journal of Botany*, 56(1), 1. doi: 10.1071/bt07151
- Baldocchi, D. (2014). Measuring fluxes of trace gases and energy between ecosystems and the atmosphere - the state and future of the eddy covariance method. *Global Change Biology*, 20(12), 3600–3609. doi: 10.1111/gcb.12649
- Blackburn, D. A. (2017). Investigations of carbon and water fluxes in a Sierra Nevada Meadow. Retrieved December 01, 2020, from <https://geog.sfsu.edu/thesis/investigations-biomicrometeorology-restored-montane-meadow>
- Blackburn, D. A., Oliphant, A. J., & Davis, J. D. (2021). Carbon and water exchanges in a mountain meadow ecosystem, Sierra Nevada, California. *Wetlands*, 41(3). <https://doi.org/10.1007/s13157-021-01437-2>
- Bouwes, N. (2020). BDA Stream Restoration. Retrieved October 13, 2020, from <https://www.beaverinstitute.org>
- Burba, G. (2013). *Eddy covariance method for scientific, industrial, agricultural, and regulatory applications: A field book on measuring ecosystem gas exchange and areal emission rates*. LI-COR Biosciences.

- Chambers J.C., Tausch R.J., Korfmacher J.L., Miller J.R. & Jewett D.G. (2004). Effects of geomorphic processes and hydrologic regimes on riparian vegetation. In: Great Basin Riparian Ecosystems— Ecology, Management and Restoration (eds. Chambers JC & (eds) JRM). Island Press Covelo, CA, USA, pp. p. 196–231
- Ciais, P., Dolman, A. J., Bombelli, A., Duren, R., Peregon, A., Rayner, P. J., Miller, C., Gobron, N., Kinderman, G., Marland, G., Gruber, N., Chevallier, F., Andres, R. J., Balsamo, G., Bopp, L., Bréon, F.-M., Broquet, G., Dargaville, R., Battin, T. J., ... Zehner, C. (2014). Current systematic carbon-cycle observations and the need for implementing a policy-relevant carbon observing system. *Biogeosciences*, *11*(13), 3547–3602.
<https://doi.org/10.5194/bg-11-3547-2014>
- Clover Valley Ranch. (2017, July 06). Retrieved May 17, 2021, from <https://chickeringco.com/portfolio-item/clover-valley-ranch/>
- Clover Valley Ranch Vegetation Monitoring (pp. 1-13, Publication). (2018). CA: Plumas contribution.
- Debinski, D. M., Jakubauskas, M. E., & Kindscher, K. (2000). Montane Meadows as Indicators of Environmental Change. *Monitoring Ecological Condition in the Western United States*, 213-225. doi:10.1007/978-94-011-4343-1_18
- Dwire, K. A., Kauffman, B., & Baham, J. E. (2006). Plant Species Distribution in Relation to Water-Table Depth and Soil Redox Potential in Montane Riparian Meadows. Retrieved December 1, 2020, from https://www.fs.fed.us/rm/pubs_other/rmrs_2006_dwire_k002.pdf
- Fisher, J. I., & Mustard, J. F. (2007). Cross-scalar satellite phenology from ground, landsat, and Modis Data. *Remote Sensing of Environment*, *109*(3), 261–273.
<https://doi.org/10.1016/j.rse.2007.01.004>
- Gilbert, G. K. (1917). Hydraulic-mining débris in the Sierra Nevada: Gilbert ... Retrieved December 1, 2020, from <https://www.amazon.com/Hydraulic-mining-d%C3%A9bris-Sierra-Nevada-Gilbert/dp/B003QCJ5XM>
- Goldfarb, B. (2018). Beaver dams without beavers? Artificial logjams are a popular but controversial restoration tool. *Science*. doi:10.1126/science.aau3887
- Hammersmark C.T., Rains M.C. & Mount J.F. (2008). Quantifying the hydrological effects of stream restoration in a montane meadow, northern California, USA. *River Research and Applications*, *24*, 735-753.

- Hirota, M., Zhang, P., Gu, S., Shen, H., Kuriyama, T., Li, Y., & Tang, Y. (2010). Small-scale variation in ecosystem CO₂ fluxes in an alpine meadow depends on plant biomass and species richness. *Journal of Plant Research*, 123(4), 531–541. doi: 10.1007/s10265-010-0315-8
- Huning, L.S., AghaKouchak, A. (2018). Mountain snowpack response to different levels of warming. *PNAS*. 115 (43), 10932–10937.
- Hunsaker, C., Whitaker, T., & Bales, R. (2012, February 28). Snowmelt Runoff and Water Yield Along Elevation and Temperature Gradients in California's Southern Sierra Nevada¹. Retrieved December 01, 2020, from <https://onlinelibrary.wiley.com/doi/10.1111/j.1752-1688.2012.00641.x>
- James, A. (1994). Channel Changes wrought by gold mining: Northern Sierra Nevada, California. Retrieved December 5, 2020, from http://people.cas.sc.edu/ajames/Research/Pubs/1994%20James%20_AWRA.pdf
- Kayranli, B., Scholz, M., Mustafa, A., & Hedmark, Å. (2010). "Carbon storage and fluxes within freshwater wetlands: a critical review." *Wetlands* 30, no. 1: 111-124.
- Keeley J.E., Lubin D. & Fotheringham C. (2003). Fire and grazing impacts on plant diversity and alien plant invasions in the southern Sierra Nevada. *Ecological Applications*, 13, 1355-1374.
- Keenan, T. F., Baker, I., Barr, A., Ciais, P., Davis, K., Dietze, M., Dragoni, D., Gough, C. M., Grant, R., Hollinger, D., Hufkens, K., Poulter, B., McCaughey, H., Raczka, B., Ryu, Y., Schaefer, K., Tian, H., Verbeeck, H., Zhao, M., & Richardson, A. D. (2012). Terrestrial biosphere model performance for inter-annual variability of land-atmosphere CO₂ exchange. *Global Change Biology*, 18(6), 1971–1987. <https://doi.org/10.1111/j.1365-2486.2012.02678.x>
- Knox, S. H., Sturtevant, C., Matthes, J. H., Koteen, L., Verfaillie, J., & Baldocchi, D (2015). "Agricultural peatland restoration: effects of land use change on greenhouse gas (CO₂ and CH₄) fluxes in the Sacramento-San Joaquin Delta." *Global change biology* 21, no. 2: 750-765.
- Liu, Y., & Wu, C. (2020). Understanding the role of phenology and summer physiology in controlling net ecosystem production: A multiscale comparison of satellite, PhenoCam and Eddy Covariance Data. *Environmental Research Letters*, 15(10), 104086. <https://doi.org/10.1088/1748-9326/abb32f>

- Lord M.L., Jewett D.G., Miller J.R., Germanoski D. & Chambers J.C. (2011). Hydrologic Processes Influencing Meadow Ecosystems. USDA Forest Service General Technical Report RMRS-GTR258, 44-67
- Loheide S.P., II & Gorelick S.M. (2007). Riparian hydroecology: A coupled model of the observed interactions between groundwater flow and meadow vegetation patterning. *Water Resources Research*, 43.
- Loheide S.P., II & Lundquist J.D. (2009). Snowmelt-induced diel fluxes through the hyporheic zone. *Water Resources Research*, 45
- Loheide S.P., Deitchman R.S., Cooper D.J., Wolf E.C., Hammersmark C.T. & Lundquist J.D. (2009). A framework for understanding the hydroecology of impacted wet meadows in the Sierra Nevada and Cascade Ranges, California, USA. *Hydrogeology Journal*, 17, 229-246.
- Lowry, C. S., Loheide, S. P., Moore, C. E., & Lundquist, J. D. (2011). Groundwater controls on vegetation composition and patterning in mountain meadows. *Water Resources Research*, 47(10). doi:10.1029/2010wr010086
- Luo, Y., El-Madany, T. S., Filippa, G., Ma, X., Ahrens, B., Carrara, A., Gonzalez-Cascon, R., Cremonese, E., Galvagno, M., Hammer, T. W., Pacheco-Labrador, J., Martín, M. P., Moreno, G., Perez-Priego, O., Reichstein, M., Richardson, A. D., Römermann, C., & Migliavacca, M. (2018). Using near-infrared-enabled digital repeat photography to track structural and physiological phenology in Mediterranean tree–grass ecosystems. *Remote Sensing*, 10(8), 1293. <https://doi.org/10.3390/rs10081293>
- Maher, S. C. (2015). Bio-micrometeorology of a Sierra Nevada montane meadow. Retrieved December 01, 2020, from <https://geog.sfsu.edu/thesis/investigations-biomicrometeorology-restored-montane-meadow>
- Mahowald, N. M., Randerson, J. T., Lindsay, K., Munoz, E., Doney, S. C., Lawrence, P., Schlunegger, S., Ward, D. S., Lawrence, D., & Hoffman, F. M. (2017). Interactions between land use change and carbon cycle feedbacks. *Global Biogeochemical Cycles*, 31(1), 96–113. <https://doi.org/10.1002/2016gb005374>
- McKelvey, K. S., & Johnston, J. D. (1992). Historical perspectives on forests of the Sierra Nevada and the transverse ranges of southern California; forest conditions at the turn of the century. Retrieved December 5, 2020, from https://www.fs.fed.us/psw/publications/documents/psw_gtr133/psw_gtr133_chap11.pdf

- Meadow Restoration. (2019). Retrieved December 01, 2020, from <https://themeadoway.ca/restoration/>
- Menke, J.W., C. Davis and P. Beesley. 1996. Rangeland assessment. Sierra Nevada Ecosystem Project: Final Report to Congress, Vol. III. Davis, CA: University of California, Davis, Centers for Water and Wildland Resources.
- Migliavacca, M., Galvagno, M., Cremonese, E., Rossini, M., Meroni, M., Sonnentag, O., Cogliati, S., Manca, G., Diotri, F., Busetto, L., Cescatti, A., Colombo, R., Fava, F., Cella, U. M. di, Pari, E., Siniscalco, C., & Richardson, A. D. (2011, June 20). *Using digital repeat photography and eddy covariance data to model grassland phenology and photosynthetic CO₂ uptake*. *Agricultural and Forest Meteorology*. Retrieved October 20, 2021, from <https://www.sciencedirect.com/science/article/pii/S0168192311001705>.
- Nagai, S., Maeda, T., Gamo, M., Muraoka, H., Suzuki, R., & Nasahara, K. N. (2011). Using digital camera images to detect canopy condition of deciduous broad-leaved trees. *Plant Ecology & Diversity*, 4(1), 79–89. <https://doi.org/10.1080/17550874.2011.579188>
- Natural Resources Conservation Service. Grizzly Peak (505) - Site Information and Reports. (2021). Retrieved October 24, 2021, from <https://wcc.sc.egov.usda.gov/nwcc/site?sitenum=505>.
- Norton, J. B., Jungst, L. J., Norton, U., Olsen, H. R., Tate, K. W., & Horwath, W. R. (2011). "Soil carbon and nitrogen storage in upper montane riparian meadows." *Ecosystems* 14, no. 8: 1217-1231.
- Novick, K. A., Walker, J., Chan, W. S., Schmidt, A., Sobek, C., & Vose, J. M. (2013). Eddy covariance measurements with a new fast-response, enclosed-path analyzer: Spectral characteristics and cross-system comparisons. *Agricultural and Forest Meteorology*, 181, 17–32. <https://doi.org/10.1016/j.agrformet.2013.06.020>
- Oliphant, A. J., Blackburn, D., Maher, S., & Mousavi, S. (Writers). (2018). *Investigation of carbon cycling in Sierra Nevada meadow ecosystems*.
- Oliphant, A.J. (2012) "Terrestrial Ecosystem Atmosphere Exchange of CO₂, Water and Energy from FLUXNET; Review and MetaAnalysis of a Global insitu Observatory." *Geography Compass* 6, no. 12 (2012): 689-7
- Ponce, V., & Lindquist, D. (1990, April). MANAGEMENT OF BASEFLOW AUGMENTATION: A REVIEW1. Retrieved December 03, 2020, from <https://onlinelibrary.wiley.com/doi/abs/10.1111/j.1752-1688.1990.tb01369.x>

- Pope, K. L., Montoya, D. S., Brownlee, J. N., Dierks, J., & Lisle, T. E. (2015, March). Habitat Conditions of Montane Meadows associated with Restored and Unrestored Stream Channels of California. Retrieved November 30, 2020, from https://www.fs.fed.us/psw/publications/pope/psw_2015_pope001.pdf
- Ratliff, R. D. (1982). A meadow site classification for the Sierra Nevada, California. doi:10.2737/psw-gtr-60
- Ratliff, R. D. (1985). Meadows in the Sierra Nevada of California: State of knowledge. doi:10.2737/psw-gtr-84
- Red Clover Valley Restoration Project. (2013, March). Retrieved March, 2021, from http://www.plumascorporation.org/uploads/4/0/5/5/40554561/red_clover_poco_finalrpt.pdf
- Reed CC, Merrill AG, Drew WM et al. (2020) Montane Meadows: A Soil Carbon Sink or 867 Source? Ecosystems <https://doi.org/10.1007/s10021-020-00572-x>
- Reid, A. M., Chapman, W. K., Prescott, C. E., & Nijland, W. (2016). Using excess greenness and green chromatic coordinate colour indices from aerial images to assess lodgepole pine vigour, mortality and disease occurrence. *Forest Ecology and Management*, 374, 146–153. <https://doi.org/10.1016/j.foreco.2016.05.006>
- Richardson, A. D., Jenkins, J. P., Braswell, B. H., Hollinger, D. Y., Ollinger, S. V., & Smith, M.-L. (2007). Use of digital webcam images to track spring green-up in a deciduous broadleaf forest. *Oecologia*, 152(2), 323–334. <https://doi.org/10.1007/s00442-006-0657-z>
- Richardson, A. D., B. H. Braswell, D. Y. Hollinger, J. P. Jenkins, and S. V. Ollinger. (2009). Near-surface remote sensing of spatial and temporal variation in canopy phenology. *Ecological Applications* 19:1417-1428.
- Richardson, A. D., Anderson, R. S., Arain, M. A., Barr, A. G., Bohrer, G., Chen, G., Chen, J. M., Ciais, P., Davis, K. J., Desai, A. R., Dietze, M. C., Dragoni, D., Garrity, S. R., Gough, C. M., Grant, R., Hollinger, D. Y., Margolis, H. A., McCaughey, H., Migliavacca, M., ... Xue, Y. (2011). Terrestrial biosphere models need better representation of Vegetation PHENOLOGY: Results from the North American Carbon Program Site Synthesis. *Global Change Biology*, 18(2), 566–584. <https://doi.org/10.1111/j.1365-2486.2011.02562.x>
- Sacks, W. J., Schimel, D. S., & Monson, R. K. (2006). Coupling between carbon cycling and climate in a high-elevation, Subalpine Forest: A model-data fusion analysis. *Oecologia*, 151(1), 54–68. <https://doi.org/10.1007/s00442-006-0565-2>

- Schilling K.E., Zhang Y.K. & Drobney P. (2004). Water table fluctuations near an incised stream, Walnut Creek, Iowa. *Journal of Hydrology*, 286, 236-248.
- Syednasrollah, B., Young, A. M., Hufkens, K., Milliman, T., Friedl, M. A., Frohking, S., & Richardson, A. D. (2019). Tracking vegetation phenology across diverse biomes using ... Retrieved December 1, 2020, from https://bnasr.github.io/papers/Syednasrollah_et_al_2019_SciData.pdf
- Sierra Meadows: Historical Impact, Current Status and Trends, and Data Gaps. (2007). Retrieved December 1, 2020, from <https://watershed.ucdavis.edu/pdf/SierraMeadows-2007.pdf>
- Sierra Nevada Restoration. (2018). Retrieved December 01, 2020, from <https://www.watereducation.org/aquapedia/sierra-nevada>
- Sonnentag, O., Hufkens, K., Teshera-Sterne, C., Young, A. M., Friedl, M., Braswell, B. H., Milliman, T., O'Keefe, J., & Richardson, A. D. (2012). Digital repeat photography for phenological research in Forest Ecosystems. *Agricultural and Forest Meteorology*, 152, 159–177. <https://doi.org/10.1016/j.agrformet.2011.09.009>
- Stucky, B., Guralnick, R., Deck, J., Denny, E., Bolmgren, K., & Walls, R. (2018, April 04). The Plant Phenology Ontology: A New Informatics Resource for Large-Scale Integration of Plant Phenology Data. Retrieved December 01, 2020, from <https://www.frontiersin.org/articles/10.3389/fpls.2018.00517/full>
- Taskey, R. D. (1995). Natural Resources Conservation Service. Retrieved December 01, 2020, from <https://www.nrcs.usda.gov/wps/portal/nrcs/surveylist/soils/survey/state/?stateId=CA>
- The PHENOCAM network. *Selecting, Deploying and Maintaining Automated Digital Cameras*. The PHENOCAM network. (2018). Retrieved October 21, 2021, from <https://phenocam.sr.unh.edu/webcam/tools/>.
- The Sierra Fund. (2018). Clover Valley Ranch Monitoring and Reporting Plan. *CDFW GGRF Full Proposal*.
- Toomey, M., Friedl, M.A., Frohking, S., et al., 2015. Greenness indices from digitalcameras predict the timing and seasonal dynamics of canopy-scale photosynthesis. *Ecol. Appl.* 25, 99–111
- Torn, M. S., Biraud, S. C., Still, C. J., Riley, W. J., & Berry, J. A. (2011). Seasonal and interannual variability in ^{13}C composition of ecosystem carbon fluxes in the U.S. southern great plains. *Tellus B: Chemical and Physical Meteorology*, 63(2), 181–195. <https://doi.org/10.1111/j.1600-0889.2010.00519.x>

- Verma, S. B., Kim, J., & Clement, R. J. (1989). Carbon dioxide, water vapor and sensible heat fluxes over a tallgrass prairie. *Boundary-Layer Meteorology*, 46(1-2), 53–67. doi: 10.1007/bf00118446
- Viers, J., Purdy, S., Peek, R., Fryjoff-Hung, A., Santos, N., Katz, J., . . . Yarnell, S. (2013, January). Montane Meadows in the Sierra Nevada: Changing Hydroclimatic Conditions and Concepts for Vulnerability Assessment. Retrieved November 30, 2020, from <https://watershed.ucdavis.edu/library/montane-meadows-sierra-nevada-changing-hydroclimatic-conditions-and-concepts-vulnerability>
- Watershed Restoration on the Plumas National Forest. (2020). Retrieved December 03, 2020, from <https://www.fs.usda.gov/plumas>
- Weather Portola, California. (2020). Retrieved December 03, 2020, from <https://www.usclimatedata.com/climate/portola/california/united-states/usca0895>
- Weather Regional Climate Center, PORTOLA, CALIFORNIA. (2020). Retrieved December 03, 2020, from <https://wrcc.dri.edu/cgi-bin/cliMAIN.pl?ca7085>
- Weixelman D.A., Hill B.A., Cooper D.J., Berlow E.L., Viers J.H., Purdy S.E., Merrill A.G. & Gross S.E. (2011). A Field Key to Meadow Hydrogeomorphic Types for the Sierra Nevada and Southern Cascade Ranges in California. In. U.S. Department of Agriculture, Forest Service, Pacific Southwest Region Gen. Tech. Rep. R5-TP-034, Vallejo, California, p. 34
- Weiser, M. (2017, February 1). *Work grows to restore mountain meadows as water banks*. Water. Retrieved September 23, 2021, from <https://deeply.thenewhumanitarian.org/water/community/2017/02/03/work-grows-to-restore-mountain-meadows-as-water-banks>.
- Wetlands Restoration for Greenhouse Gas Reduction Program. (2018). Retrieved December 03, 2020, from <https://wildlife.ca.gov/Conservation/Watersheds/Greenhouse-Gas-Reduction>
- Wever, L. A., Flanagan, L. B., & Carlson, P. J. (2002). Seasonal and interannual variation in evapotranspiration, energy balance and surface conductance in a northern temperate grassland. *Agricultural and Forest Meteorology*, 112(1), 31–49. doi: 10.1016/s0168-1923(02)00041-2
- Wharton, S., Falk, M., Bible, K., Schroeder, M., & Paw U, K. T. (2012). Old-growth CO₂ flux measurements reveal high sensitivity to climate anomalies across seasonal, annual and

Decadal Time Scales. *Agricultural and Forest Meteorology*, 161, 1–14.
<https://doi.org/10.1016/j.agrformet.2012.03.007>

- Wohlfahrt, G., Hammerle, A., Haslwanter, A., Bahn, M., Tappeiner, U., & Cernusca, A. (2008). Seasonal and interannual variability of the net ecosystem CO₂ exchange of a temperate mountain grassland: Effects of weather and management. *Journal of Geophysical Research: Atmospheres*, 113(D8)
- Xu, L., & Baldocchi, D. D. (2004). Seasonal variation in carbon dioxide exchange over a Mediterranean annual grassland in California. *Agricultural and Forest Meteorology*, 123(1-2), 79–96. doi: 10.1016/j.agrformet.2003.10.004
- Yang, B. A. et al. (2009). Environmental controls on water use efficiency during severe drought in an Ozark Forest in Missouri, USA. *Global Change Biology*, 16(8), 2252–2271.
<https://doi.org/10.1111/j.1365-2486.2009.02138.x>
- Zeri, M., Anderson-Teixeira, K., Hickman, G., Masters, M., DeLucia, E., & Bernacchi, C. J. (2011). Carbon exchange by establishing biofuel crops in Central Illinois. *Agriculture, Ecosystems & Environment*, 144(1), 319–329. <https://doi.org/10.1016/j.agee.2011.09.006>
- Zhou, X., Wang, X., Zhang, S., Zhang, Y., & Bai, X. (2020). Combining phenological camera photos and modis reflectance data to predict GPP daily dynamics for Alpine Meadows on the Tibetan Plateau. *Remote Sensing*, 12(22), 3735. <https://doi.org/10.3390/rs12223735>